

## Impact of snow and cloud cover on the surface energy budget over Iceland based on HARMONIE model simulations

Nikolai Nawri



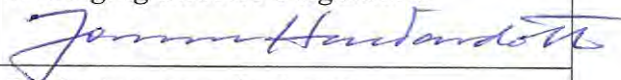
# Impact of snow and cloud cover on the surface energy budget over Iceland based on HARMONIE model simulations

---

Nikolai Nawri, Icelandic Met Office



Keypage

<b>Report no.:</b> VÍ 2015-006	<b>Date.:</b> September 2015	<b>ISSN:</b> 1670-8261	<b>Public</b> <input checked="" type="checkbox"/> <b>Restricted</b> <input type="checkbox"/> <b>Provision:</b>
<b>Report title / including subtitle</b> Impact of snow and cloud cover on the surface energy budget over Iceland based on HARMONIE model simulations		<b>No. of copies:</b> 4 <b>Pages:</b> 42	
<b>Author(s):</b> Nikolai Nawri		<b>Managing director:</b> Jórunn Harðardóttir	
		<b>Project manager:</b> Halldór Björnsson	
		<b>Project number:</b> 5818-0-0001	
<b>Project phase:</b>		<b>Case number:</b> 2015-240	
<b>Report contracted for:</b>			
<b>Prepared in cooperation with:</b>			
<b>Summary:</b> In this study, the sensitivity of the HARMONIE mesoscale weather prediction model to changes in snow and cloud cover is investigated, based on case studies of three individual days in the late summer and early autumn of 2012. The three days were associated with different large-scale weather patterns, and characterised by different cloud conditions over Iceland, which were generally well simulated by HARMONIE. At local noon, the net downward total energy flux is positive across the model domain. It is largely unaffected by cloud conditions, but significantly depends on surface type. By contrast, longwave radiation fluxes are less dependent on the presence or absence of snow on the ground, and more on cloud conditions.			
<b>Keywords:</b> HARMONIE mesoscale model Radiation fluxes, Heat fluxes Surface energy balance, Iceland		<b>Managing director's signature:</b> 	
		<b>Project manager's signature:</b>	
		<b>Reviewed by:</b> Bolli Pálmason, SG	



# Contents

<b>1 Introduction</b> .....	7
<b>2 Test cases</b> .....	8
27 July 2012 .....	8
3 August 2012 .....	10
3 September 2012 .....	12
<b>3 Radiation fluxes at the surface</b> .....	16
<b>4 Heat fluxes at the surface</b> .....	21
<b>5 Net energy budget at the surface</b> .....	26
<b>6 Impact of glaciers on surface winds</b> .....	37
<b>7 Conclusion</b> .....	40

## List of Figures

1	Weather conditions on 27 July 2012 at 12 UTC .....	9
2	Weather conditions on 3 August 2012 at 12 UTC .....	11
3	Weather conditions on 3 September 2012 at 12 UTC .....	13
4	Hourly rainfall during 3 September 2012.....	14
5	Distribution of low-, medium-, and high-level cloud cover .....	15
6	Net downward shortwave radiation flux at the surface .....	18
7	Net downward longwave radiation flux at the surface.....	19
8	Net downward total radiation flux at the surface.....	20
9	Upward sensible heat flux from the ground.....	22
10	Air temperature at 2 mAGL.....	23
11	Upward latent heat flux from the ground .....	25
12	Net downward energy flux at the surface, without snowmelt .....	27
13	Net downward energy flux at the surface, with snowmelt .....	29
14	Average downward energy fluxes on 27 July 2012.....	31
15	Average downward energy fluxes on 27 July 2012 over the ocean .....	32
16	Average downward energy fluxes on 3 August 2012 .....	34
17	Average downward energy fluxes on 3 September 2012.....	35
18	Relative humidity at 2 mAGL .....	36
19	Differences in mean sea level air pressure.....	38
20	Differences in the meridional wind component at 10 mAGL.....	39



# 1 Introduction

The goal of this study is to establish the sensitivity of the HARMONIE mesoscale weather prediction model to changes in snow and cloud cover, with a particular emphasis on radiation and heat fluxes, as well as the overall energy balance.

The general equations and parameterisations, which constitute the core of the HARMONIE model, are described by Brousseau, Berre, Bouttier, and Desroziers (2011) and Seity et al. (2011). The model version used here is cycle 37h1.2, the same as for the operational forecast runs produced by the Icelandic Meteorological Office (IMO) between 2011 and 2014. The model domain is also the same as for the IMO operational runs, with  $300 \times 240$  horizontal grid points covering the whole of Iceland and parts of the surrounding ocean, and with a horizontal grid-point spacing of about 2.5 km in both directions. The model is run with the standard 65 vertical levels, and with a non-hydrostatic dynamic core. Radiation, turbulence, convection, and microphysics (clouds and precipitation) are determined by the AROME upper air physics scheme. Surface and soil processes are described by the external single-layer coupled surface scheme SURFEX. Initial and boundary conditions are provided by ERA-Interim reanalyses, with a boundary data interval of six hours. The lateral boundaries of the HARMONIE model have a relaxation zone of 10 grid points, wherein the coarse-resolution outer data from the host model is blended with the high-resolution data within the dependent model domain. At the upper boundary, defined as the 10-hPa isobaric surface, vertical velocity is set to zero.

Since the purpose of this study is to conduct a sensitivity rather than a climatological analysis, only three individual days in the late summer and early autumn of 2012 are being considered: 27 July, 3 August, and 3 September. As discussed below, these dates were associated with different large-scale weather patterns, and characterised by different cloud conditions over Iceland.

For each case, four model experiments were performed: two forecast runs, separated in start time by one day (1 and 2 days prior to the days under consideration), for two different initial snow covers.

For the “no snow” runs, variable snow depth in the initial boundary data is set to zero throughout the model domain. This effectively removes the glaciers since, in the current setup of HARMONIE, “permanent snow” in the model has neither radiative nor thermodynamic properties of either snow or ice. For the “snow on glaciers” runs, initial snow depth is determined by placing 50 cm of snow water equivalent (SWE) (or  $500 \text{ kg m}^{-2}$  of snow) on top of the permanent snow regions, as defined by the model glacier mask. The “snow on glaciers” runs are used for most of the analysis presented here, whereas the “no snow” runs are used in the last section, to determine the impact of glaciers on the thermodynamic properties of the boundary-layer atmosphere, and particularly on the low-level wind field.

The earlier of the two runs for each case and initial snow cover serves as a control for the later run. By comparing forecast hours 0 – 48 of the later run, with forecast hours 24 – 72 of the earlier run, it was found that, for all three cases, the atmospheric component of the model loses memory of the initial conditions within 12 – 24 hours. Therefore, forecast hours 24 – 48 of the later runs are used here, during which all effects of the atmospheric initialisation process have been eliminated, and the model has completely adjusted to its own internal reality.

## 2 Test cases

This section provides a brief summary of the large-scale atmospheric conditions on the three days considered in this study, with an emphasis on clouds and precipitation. It is shown that the weather over Iceland on these days was generally well simulated by HARMONIE, although for the first two cases, small precipitation events and mid-level cloud cover were underestimated.

### 27 July 2012

Throughout the day, Iceland was situated between a weak low moving east over the Faroe and Shetland Islands, and a ridge extending north from a high over the mid-latitude North Atlantic to Greenland (see Figure 1 for the conditions at 12 UTC, based on ERA-Interim reanalyses, as well as manned observations and measurements from the synoptic station network). In the eastern part of the island, a few slight rain showers occurred at night and in the morning. Otherwise, weather conditions were dry. Winds were weak to intermediate ( $2 - 11 \text{ m s}^{-1}$ ) from prevailing northerly to northeasterly directions.

As mentioned in the introduction, ERA-Interim reanalyses were used as initial and boundary conditions for the HARMONIE model simulations. However, near the coast, the manned observations of precipitation and cloud cover provide an independent dataset for comparison with the model results.

The HARMONIE results for low-, medium-, and high-level cloud cover, on a reduced model grid, including only every 10th grid point, are shown in Figure 5. The values are horizontal averages, taking into account the neighbouring 5 grid points. In broad terms, model simulations and observations agree on clouds having been present over the eastern half of the island at 0 UTC, with clear skies in the west. Then, over the course of the day, the sky cleared in the east. However, nighttime showers in the east are not simulated by the model, and there are differences in the types of clouds present. Based on manned observations, cumulus, stratocumulus, or cumulonimbus were most prevalent at low levels, usually occurring together with altocumulus. At a few locations, stratus was observed together with altostratus. This combination of cloud layers is not reflected in the model, where mid-level cloud cover, over the land, is underrepresented.



### **3 August 2012**

Similar to 27 July, a ridge was situated over the central part of the North Atlantic, blocking the formation and eastward movement of lows over the western part of the ocean (see Figure 2 for the conditions at 12 UTC). However, over the course of the day, a weak low formed over Iceland, and cloud cover, at least near the coast, was greater than during the previous case. Based on manned observations at a few coastal locations, slight intermittent drizzle occurred until around noon, which was not simulated by the model. As seen previously, mid-level clouds were underestimated by the model on 27 July. This is even more noticeable on 3 August, when the model simulated no mid-level cloud cover at all (see again Figure 5). Throughout the day, model cloud conditions are characterised primarily by low clouds, whereas a layer of altocumulus and altostratus was observed at several locations. However, consistent with manned observations, the increased presence of high-level clouds was simulated well during the second half of the day. Winds were generally weak ( $2 - 6 \text{ m s}^{-1}$ ) from variable directions.



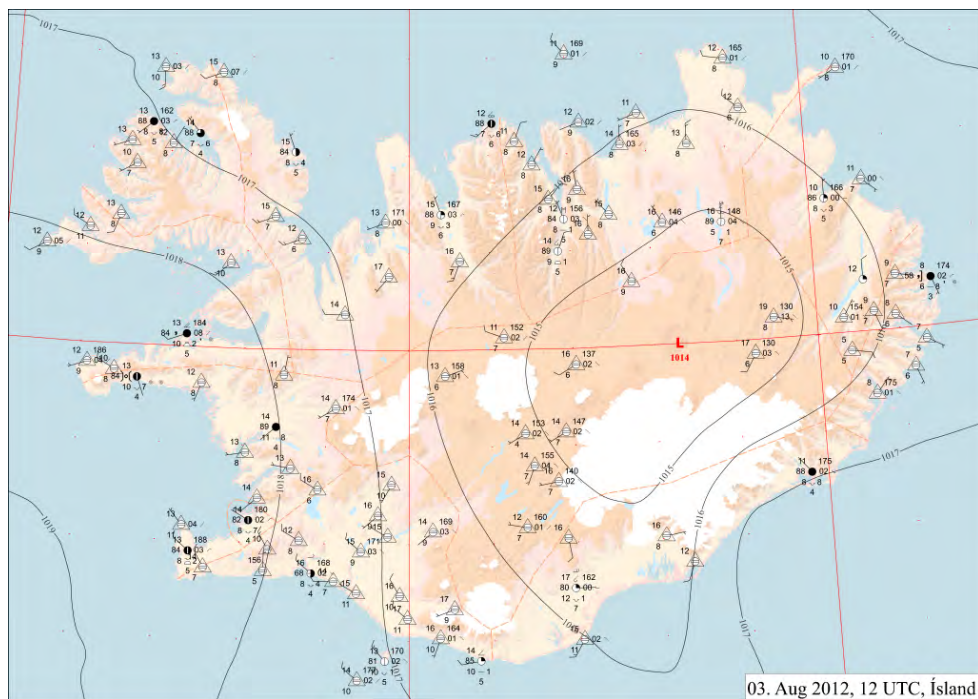
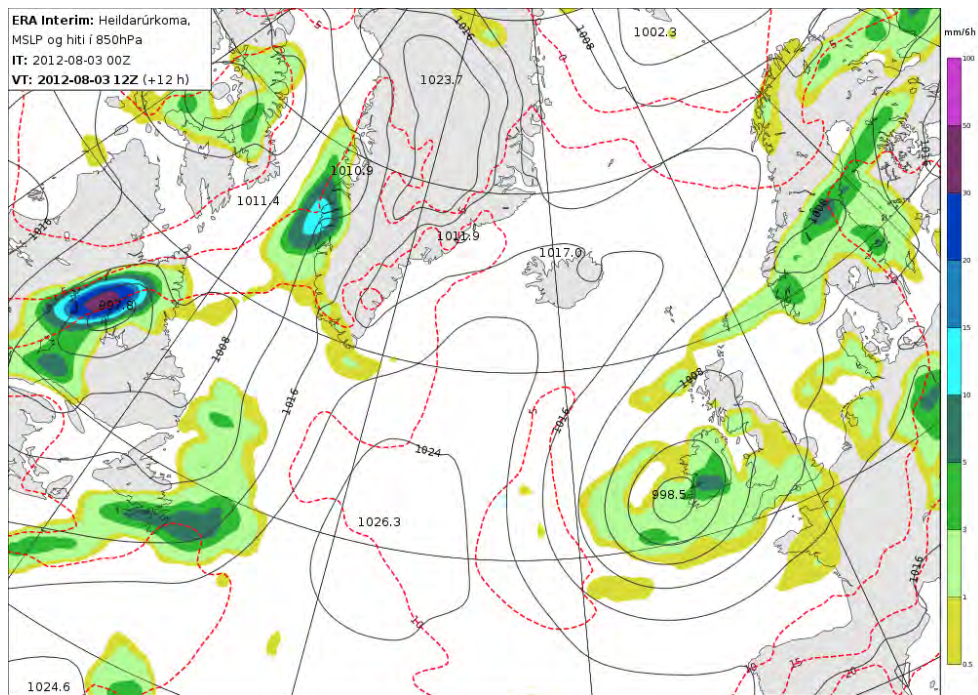


Figure 2. Weather conditions on 3 August 2012 at 12 UTC (local time). Top panel: large-scale analysis based on ERA-Interim reanalysis data, with mean sea level air pressure (black contours), temperature at 850 hPa (dashed red contours), and 6-hourly accumulated precipitation (coloured contours). Bottom panel: manned and automated surface observations over Iceland.

### 3 September 2012

Weather conditions on that day were determined by an intensifying low-pressure system, which moved across Iceland from southwest to northeast (see Figure 3 for the conditions at 12 UTC). The sky was mostly overcast, based both on model simulations as well as observations. Contrary to the two previous cases, the model simulated dense cloud cover at all three levels, consistent with manned observations. Therefore, on 3 September, there was a greater horizontal extent, as well as a greater vertical thickness of the cloud cover over land. Based on manned observations, low-level cloud cover was dominated by stratus and stratocumulus, whereas at mid-levels, altostratus was most prevalent. Near the coast, where manned observations are available for comparison, precipitation was well simulated by the model (see Figure 4). The highest precipitation occurred over the ocean and in that part of the coastal zone, with strong onshore winds. In the morning, the most intense band of precipitation was situated over the outlying peninsulas in the west. As the low moved over the island, the region with the heaviest precipitation shifted south and then cyclonically along the coast to the northeast. Winds were intermediate to strong ( $3 - 16 \text{ m s}^{-1}$ ), turning from prevailing southerly to prevailing northerly directions over the course of the day.

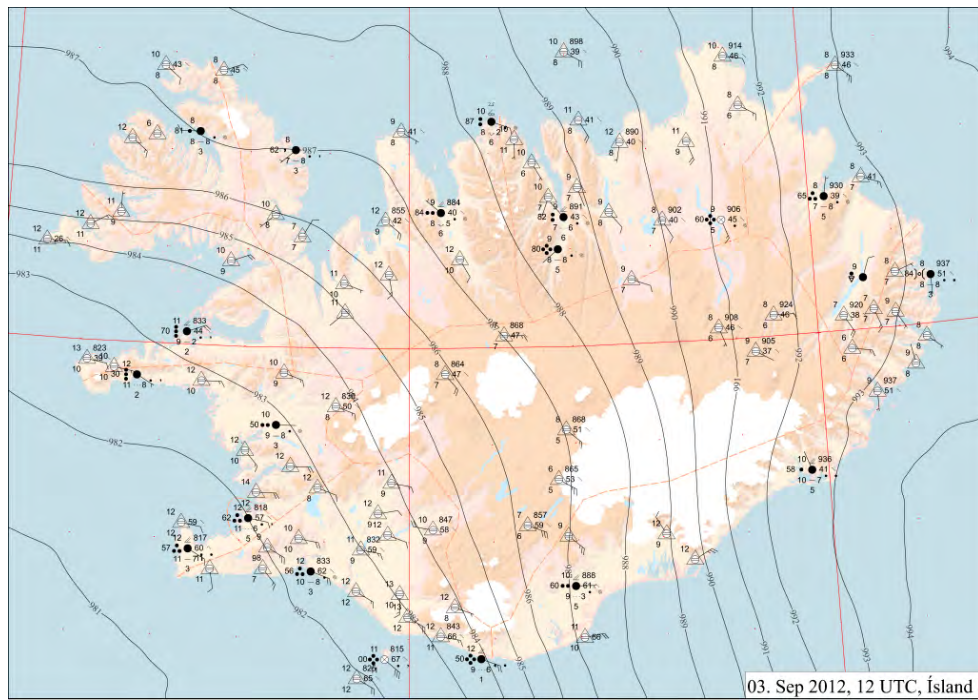
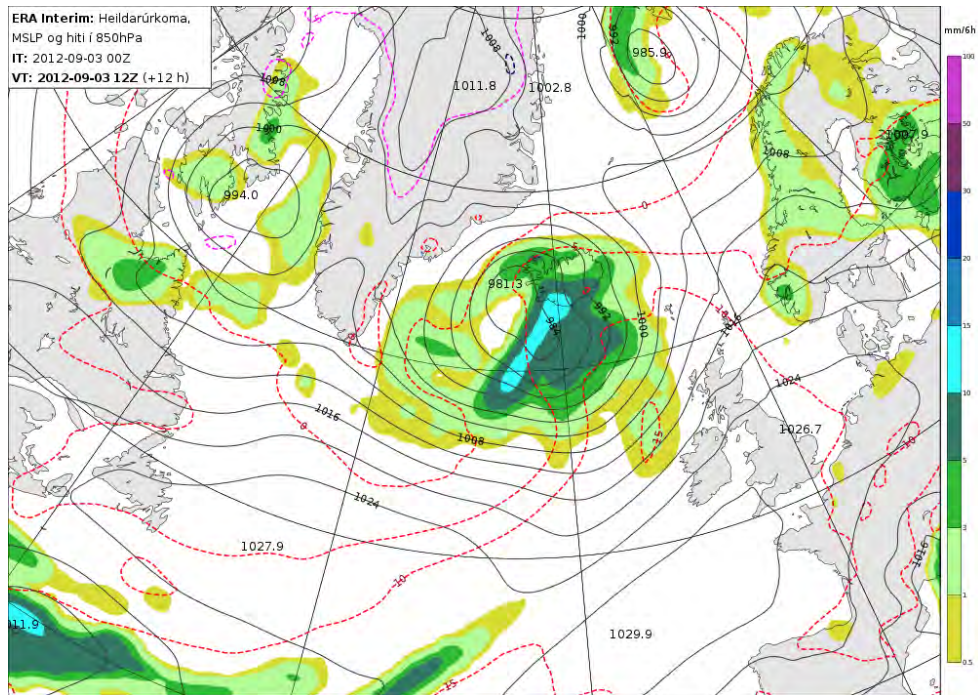


Figure 3. Weather conditions on 3 September 2012 at 12 UTC (local time). Top panel: large-scale analysis based on ERA-Interim reanalysis data, with mean sea level air pressure (black contours), temperature at 850 hPa (dashed red contours), and 6-hourly accumulated precipitation (coloured contours). Bottom panel: manned and automated surface observations over Iceland.



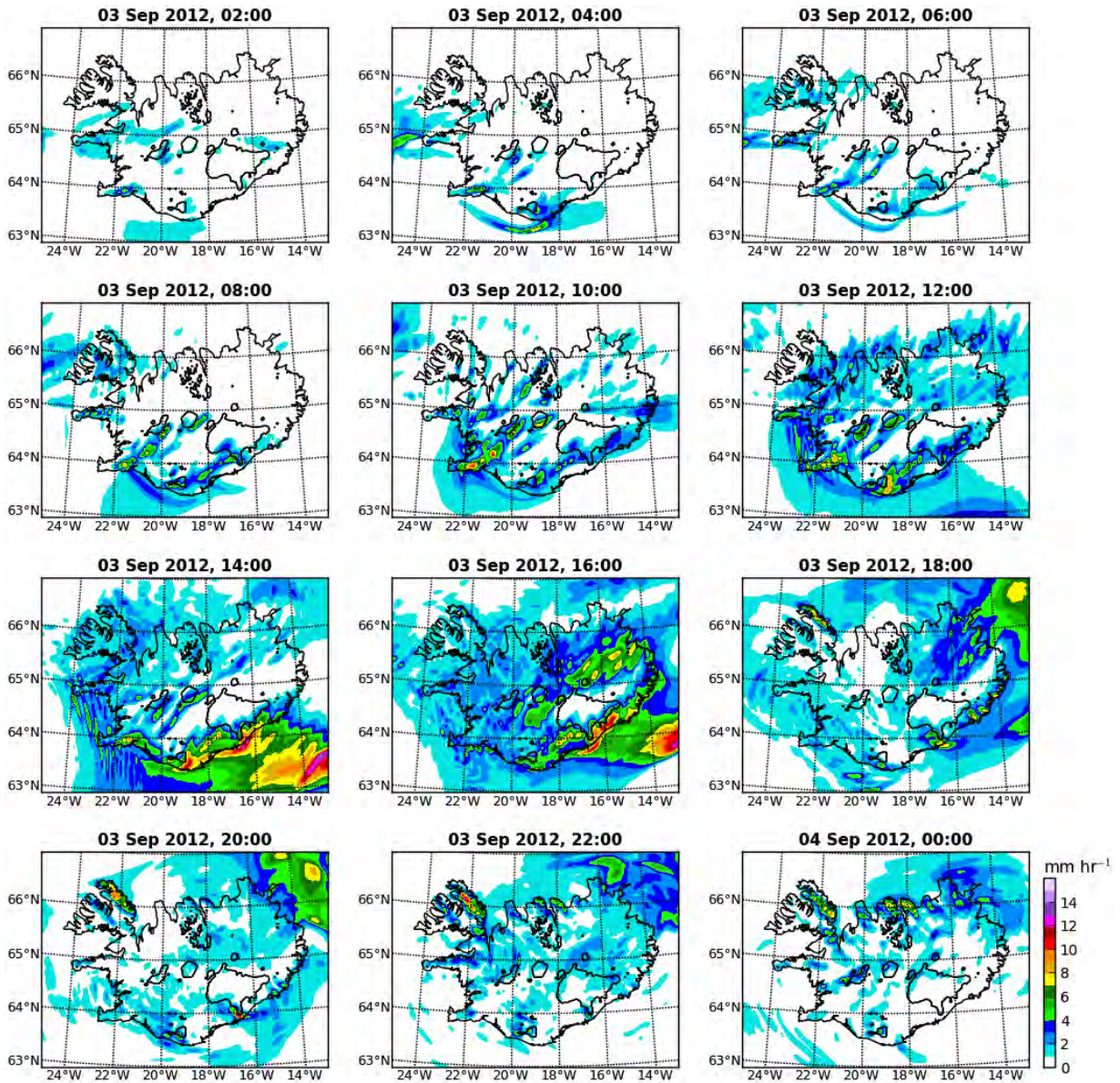


Figure 4. Hourly rainfall during 3 September 2012, based on HARMONIE model simulations. Times are in UTC (local time).



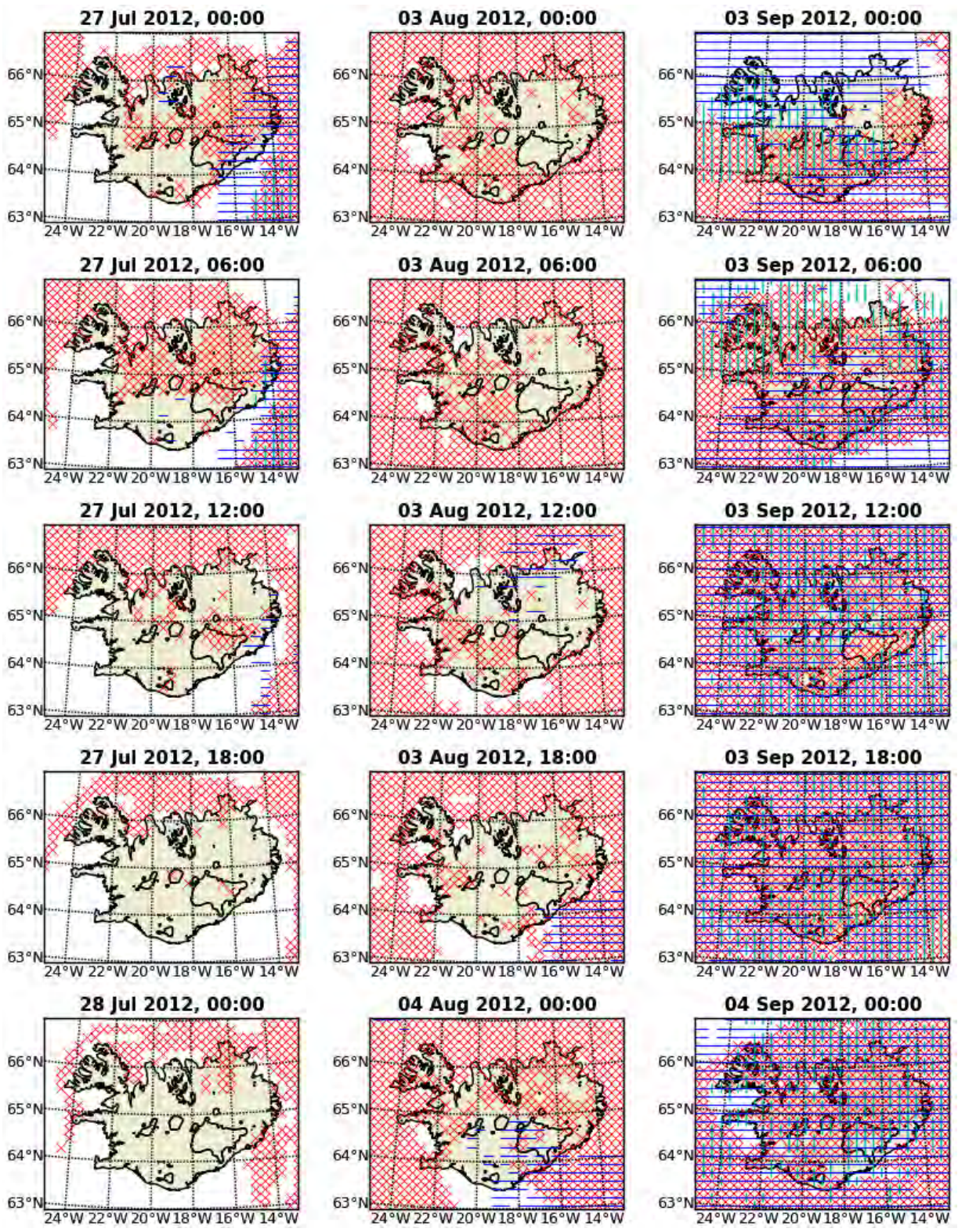


Figure 5. Distribution of low- (red crosses), medium- (green vertical lines), and high-level (blue horizontal lines) cloud cover of at least 90%, based on HARMONIE model simulations. Terrain elevation contour lines are drawn at 1000 mASL, indicating roughly the extent of the glaciers.



### 3 Radiation fluxes at the surface

With increasing time past the summer solstice (20 June 2012), the solar energy per unit area received at the Earth’s surface, for the same cloud and snow conditions, decreases due to the shorter days and lower sun altitude angles. The characteristics of the solar cycle, for the three days considered here, are listed in Table 1. Changes in orbital parameters are mainly significant between the last and the previous two cases, with a drop in noontime solar intensity, defined as the sine of the sun altitude angle, by 14–17%. This difference needs to be taken into account when comparing shortwave radiation fluxes between the different cases.

The diurnal cycles of net shortwave radiation flux on the three days are shown in Figure 6. As is to be expected, the net downward (incident minus outgoing) total (direct and diffuse) shortwave radiation flux at the surface is largest around solar noon, under clear skies, and over low-albedo surfaces. For the cases discussed here, the highest values are found on 27 July over the ocean south and west of Iceland. Differences in net shortwave flux due to differences in cloud cover (compare with Figure 5) are especially noticeable on 27 July and 3 August around (local) noon when, off the south and southwest coast, the net flux under clear skies is increased by up to  $300 \text{ W m}^{-2}$ , compared with neighbouring cloud-covered regions. Although, generally, there was a more extensive cloud cover over the land on 3 August than on 27 July, over the glaciers, the sky was mostly cloud-free during sunshine hours, whereas on 27 July, a low-level cloud layer existed over parts of the glaciers. Comparing these two days, the shortwave radiation balance at noon over the northern part of Vatnajökull is lower by about  $200 \text{ W m}^{-2}$  on 27 July with overcast conditions, than on 3 August under clear skies. Differences in net shortwave radiation flux between snow-free and snow-covered regions, under clear skies, are of the same magnitude as differences between overcast and clear-sky conditions over the same surface type. At around noon, across the southern edge of Vatnajökull on 27 July, and across the northern edge on 3 August, for example, the net shortwave radiation flux increases from  $300 \text{ W m}^{-2}$  over the glacier to  $500 \text{ W m}^{-2}$  over the snow-free land.

The diurnal cycles of net downward longwave radiation flux for the three cases are shown in Figure 7. Longwave radiation losses are highest with clear skies and over warm (dark) surfaces, such as the rocky terrain on Snæfellsnes and in the Westfjords, where they can reach up to  $180 \text{ W m}^{-2}$ . Of the two factors that determine the net longwave radiation balance, differences in cloud conditions, especially with low clouds, have the largest impact. A comparison between Figures 5 and 7 shows that, even with a single layer of low clouds, longwave radiation losses

*Table 1. Time of sunrise, sunset, and length of day at  $65^\circ\text{N}$ ,  $19^\circ\text{W}$ , and at mean sea level. Also given are local time and sun altitude angle at solar noon (source: <http://susdesign.com/sunangle/>). Normalised solar intensity is given as the sine of the altitude angle. Absolute incident solar intensity at the top of the atmosphere is obtained by multiplication with  $1360 \text{ W m}^{-2}$ .*

	Rise [UTC]	Set [UTC]	Length [hrs]	Noon [UTC]	Altitude [deg]	Intensity
27 Jul 2012	03:58	22:46	18:48	13:22	44.05	0.70
3 Aug 2012	04:22	22:21	17:59	13:22	42.32	0.67
3 Sep 2012	06:03	20:27	14:24	13:15	32.30	0.53

are limited to about  $50 \text{ W m}^{-2}$  or less, compared with losses of  $80 \text{ W m}^{-2}$  or more over neighbouring cloud-free regions. The conditions around midnight, off the southeast coast on 27 July, and along the north coast on 3 September, clearly show the limited ability (in the model) of even a complete high-level cloud cover to affect the longwave radiation balance at the surface. Mid-level clouds are usually simulated together with clouds at low-levels. However, around midnight on 3 September, north of the edge of the low-level cloud cover, there are indications that longwave radiation losses are significantly reduced by a complete mid-level cloud cover. By contrast with the effects of cloud cover, as seen clearly at midnight and in the early morning of 27 July, the difference in the longwave radiation balance between neighbouring snow-covered and snow-free surfaces, under either overcast or clear conditions, is negligible. During the day, the impact of surface type is slightly increased, but generally less than  $30 \text{ W m}^{-2}$  between neighbouring snow-covered and snow-free regions. Longwave radiation losses can essentially be eliminated through the combined effects of a thick cloud layer and a cold (bright) snow cover. At night, the differences between land and ocean are small. However, during the day, especially with clear skies, as the land heats up faster than the surrounding water, the terrestrial longwave radiation losses can exceed those over the nearby cloud-free ocean by up to  $80 \text{ W m}^{-2}$ .

The total radiation received by the Earth's surface is determined by factors that oppositely affect the short- and longwave radiation budget. As seen above, with a clear sky, both shortwave radiation gain and longwave radiation losses are increased, compared with overcast conditions. Over snow, in comparison with snow-free ground, the higher albedo leads to increased shortwave radiation losses whereas, in summer, the lower temperatures of a snow surface may lead to reduced longwave radiation losses. The diurnal cycles of net downward total (short- plus longwave) radiation flux, for the three cases, are shown in Figure 8. At night, incoming shortwave radiation is zero, and the total radiation balance is determined exclusively by longwave radiation losses. During the day, the net total radiation flux becomes positive and increases with decreasing cloud cover. The gain in shortwave radiation under clear skies therefore outweighs the increased losses in longwave radiation. Inversely, with the dense cloud layer on 3 September, the reduction in received shortwave radiation is somewhat offset by reduced longwave radiation losses.

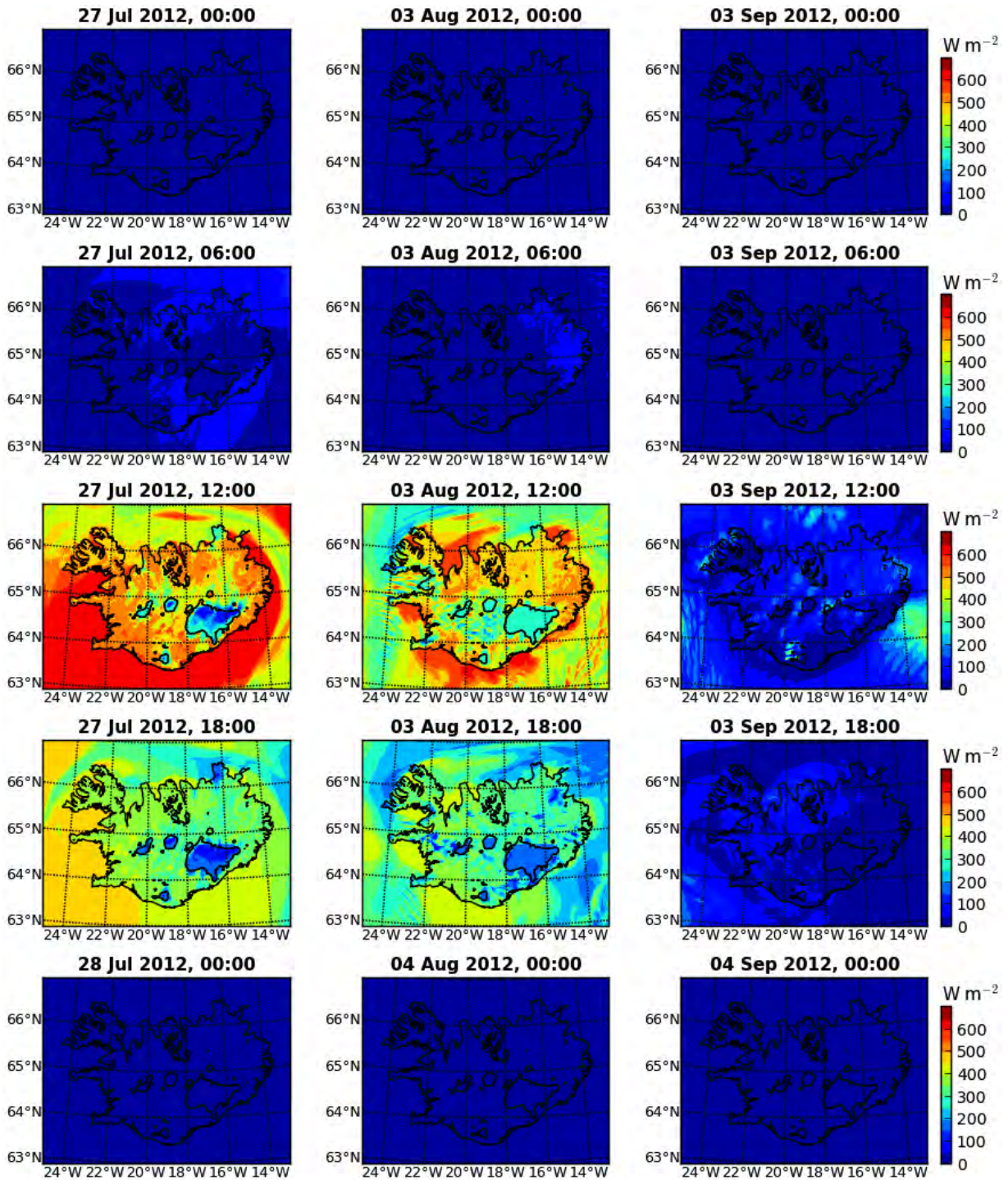


Figure 6. Net downward shortwave radiation flux at the surface, based on HARMONIE model simulations. Times are in UTC (local time). Terrain elevation contour lines are drawn at 1000 mASL, indicating roughly the extent of the glaciers.



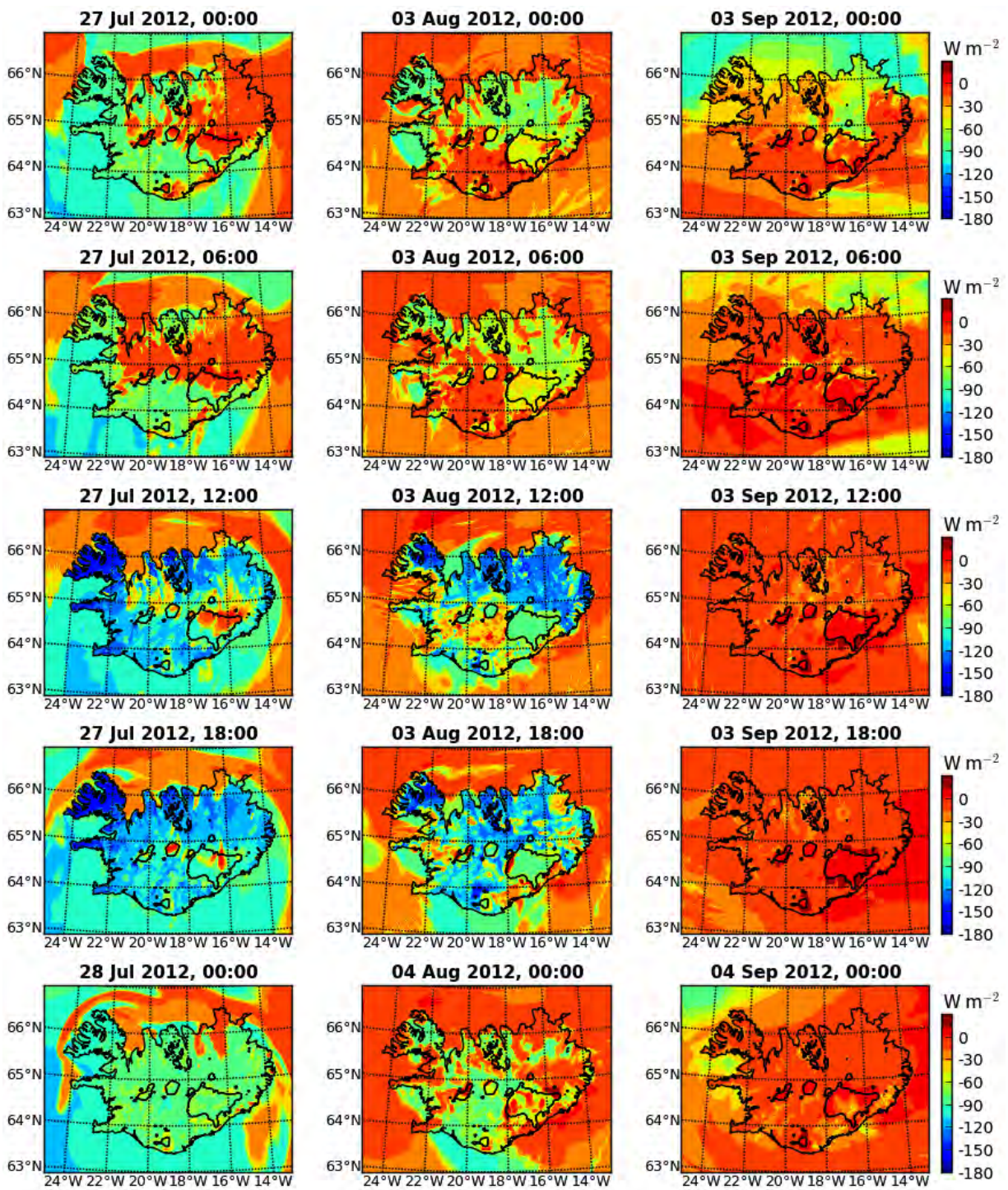


Figure 7. Net downward longwave radiation flux at the surface, based on HARMONIE model simulations.



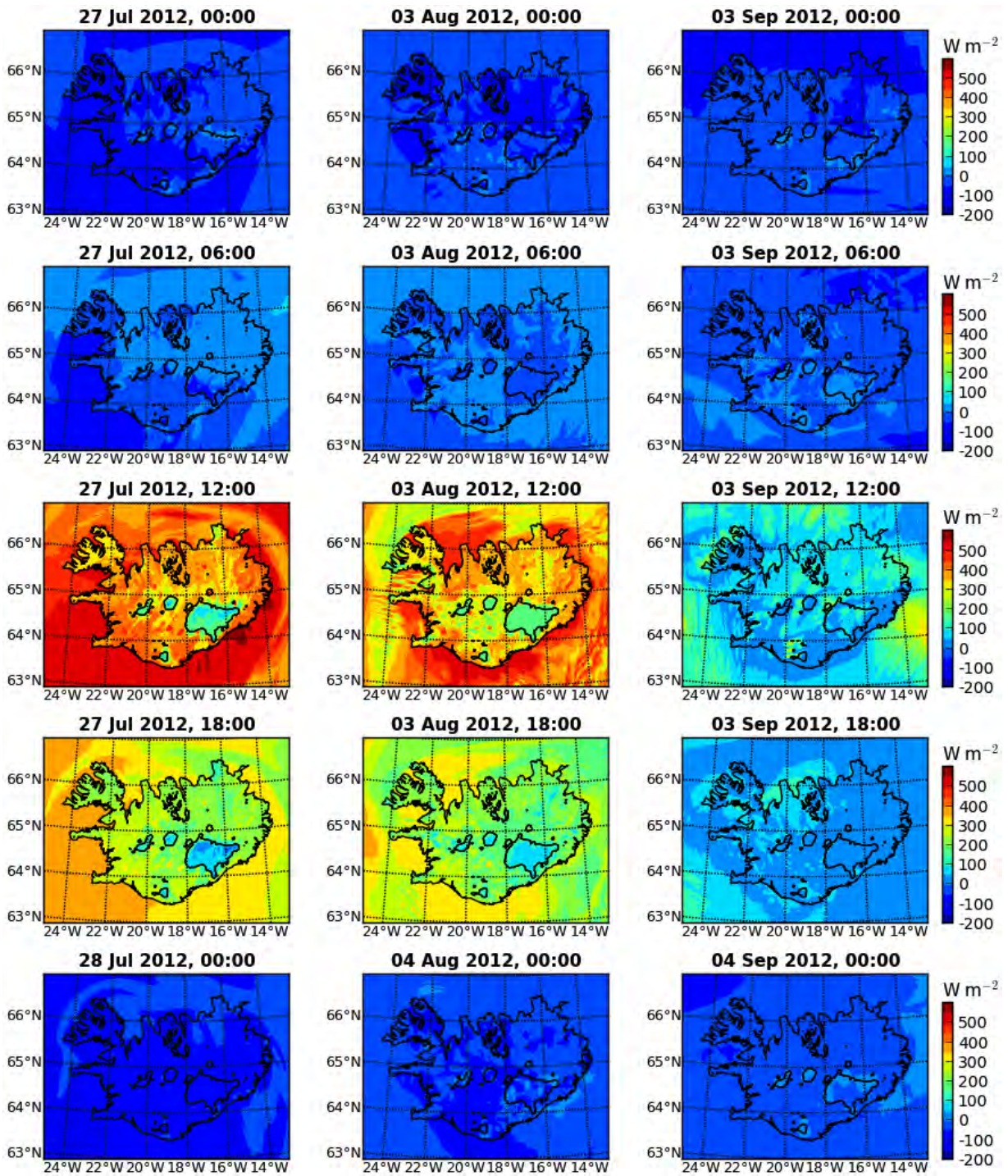


Figure 8. Net downward total radiation flux at the surface, based on HARMONIE model simulations.

## 4 Heat fluxes at the surface

As seen in the previous section, in late summer and early autumn, more radiative energy is received during the day by the Icelandic land area than is lost. With a positive net total radiation balance, most of the energy received at the Earth's surface (ignoring photosynthesis for a sparsely vegetated region such as Iceland) is converted into heat, leading either to temperature changes (sensible heat), or water phase transitions (latent heat). Sensible heat is conducted down into the ground, as well as up into the lowest surface layer of the atmosphere. The reduced density of the near-surface air then causes free convection and mixing of rising air with colder air aloft. With a positive radiation budget, the most common phase transitions on the ground are evaporation and melting. Latent heat of vaporisation can be released into the atmosphere if water vapour, carried upwards in convective plumes, is cooled sufficiently to condense again, forming clouds. Latent heat of fusion is retained by meltwater until it refreezes. Under sunny, cold, and dry conditions, sublimation of snow may also contribute to latent heat fluxes from the ground to the atmosphere.

In HARMONIE, surface sensible heat flux is defined within the context of soil processes, and is related to changes in ground, rather than atmospheric temperature. Therefore, in the model, sensible heat flux is defined positive, if heat is transferred from the atmosphere to the ground. This is in contrast with latent heat fluxes, which are defined positive if directed upward. For consistency between the two types of heat fluxes, and following a common meteorological convention for non-radiative fluxes, the negatives of the original model fields of sensible heat flux are used here. Sensible heat flux in the model is accumulated over the entire forecast run, in units of  $\text{J m}^{-2}$ . Used here are hourly accumulated values, divided by 3600 seconds, resulting in average hourly fluxes in units of  $\text{W m}^{-2}$ . Surface latent heat flux is directly calculated by the model as instantaneous values in units of  $\text{W m}^{-2}$ .

The diurnal cycles of upward sensible heat flux for the three cases considered in this study are shown in Figure 9. Over the ocean, throughout 27 July, positive fluxes occur at the western edge of the low-level cloud layer southeast of Iceland (see again Figure 5). These are due to cold air advection over warmer water by strong northeasterly winds in the wake of a retreating low-pressure system (see Section 2). A similar situation exists around midnight on 4 September, at the northern edge of the low-level cloud cover north of Iceland. Over snow-free land, without a dense cloud layer as on 3 September, fluxes become positive after sunrise, due to radiative heating of the ground. The effects are most noticeable along the coast, where land–sea differences in the boundary-layer atmosphere are largest. Positive sensible heat fluxes also occur over the interior regions of Vatnajökull and Hofsjökull at around noon on 27 July, due to the cold northeasterly flow over the glaciers (see Figure 10). However, along the edges and on the other icecaps, sensible heat fluxes under clear skies are directed from the atmosphere to the snow. On 3 August, with clear skies, weak winds, and with above freezing air temperatures (rising to around  $5^{\circ}\text{C}$  over Vatnajökull), the sensible heat flux over snow remains slightly negative throughout the day. On 3 September, despite lower air temperatures but with complete cloud cover at all three levels, sensible heat fluxes over the glaciers also remain negative throughout the day.



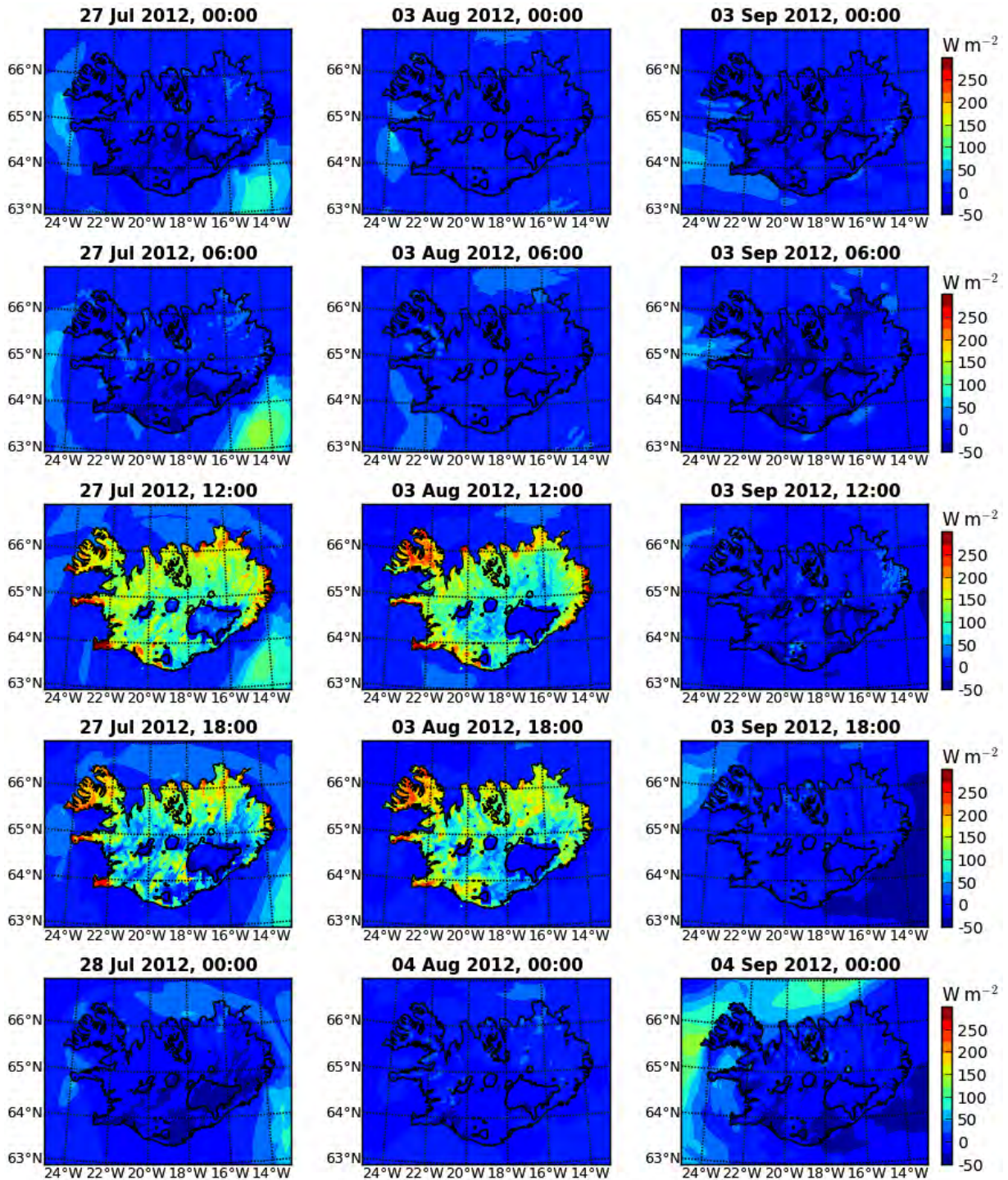


Figure 9. Upward sensible heat flux from the ground, based on HARMONIE model simulations. Times are in UTC (local time). Terrain elevation contour lines are drawn at 1000 mASL, indicating roughly the extent of the glaciers.



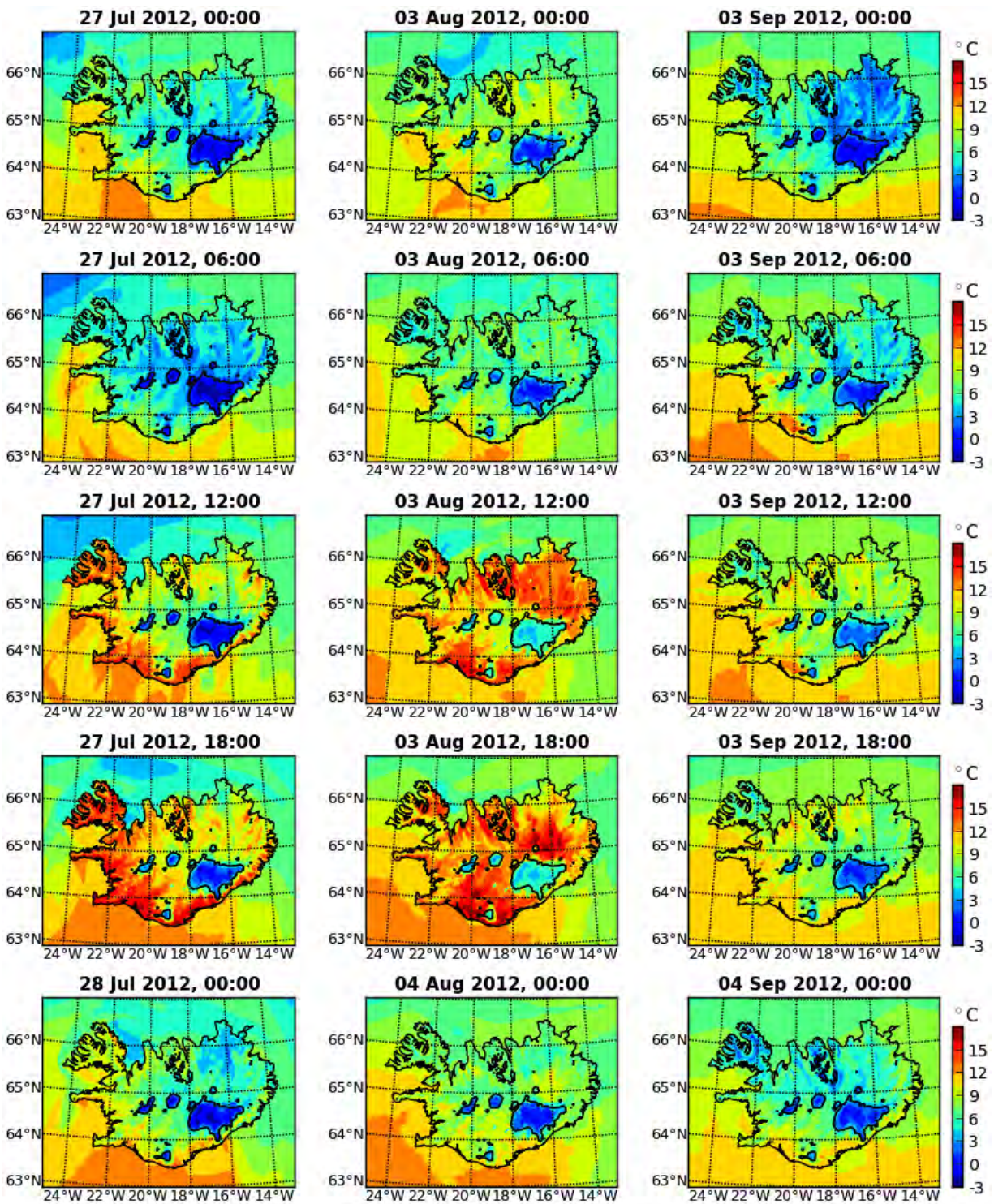


Figure 10. Air temperature at 2 mAGL, based on HARMONIE model simulations.

Upward latent heat flux from the ground, shown in Figure 11, has a similar temporal and spatial variability as sensible heat flux. Over snow, for example, latent heat fluxes into the atmosphere are also significantly reduced compared with the surrounding snow-free ground, but less so on 27 July, due to the cold and dry air flowing over the glaciers. However, there are some differences. On 27 July and 3 August, as the snow-free ground begins to heat up during the day, the highest latent heat fluxes to the atmosphere are found further inland than the highest sensible heat fluxes, in regions with the densest vegetation cover. During the night and early morning of 3 September, with cold east-southeasterly offshore winds, latent heat fluxes over the ocean west of Iceland exceed sensible heat fluxes in that region. With a thick cloud cover, throughout the day, this is also true over the snow-free land.



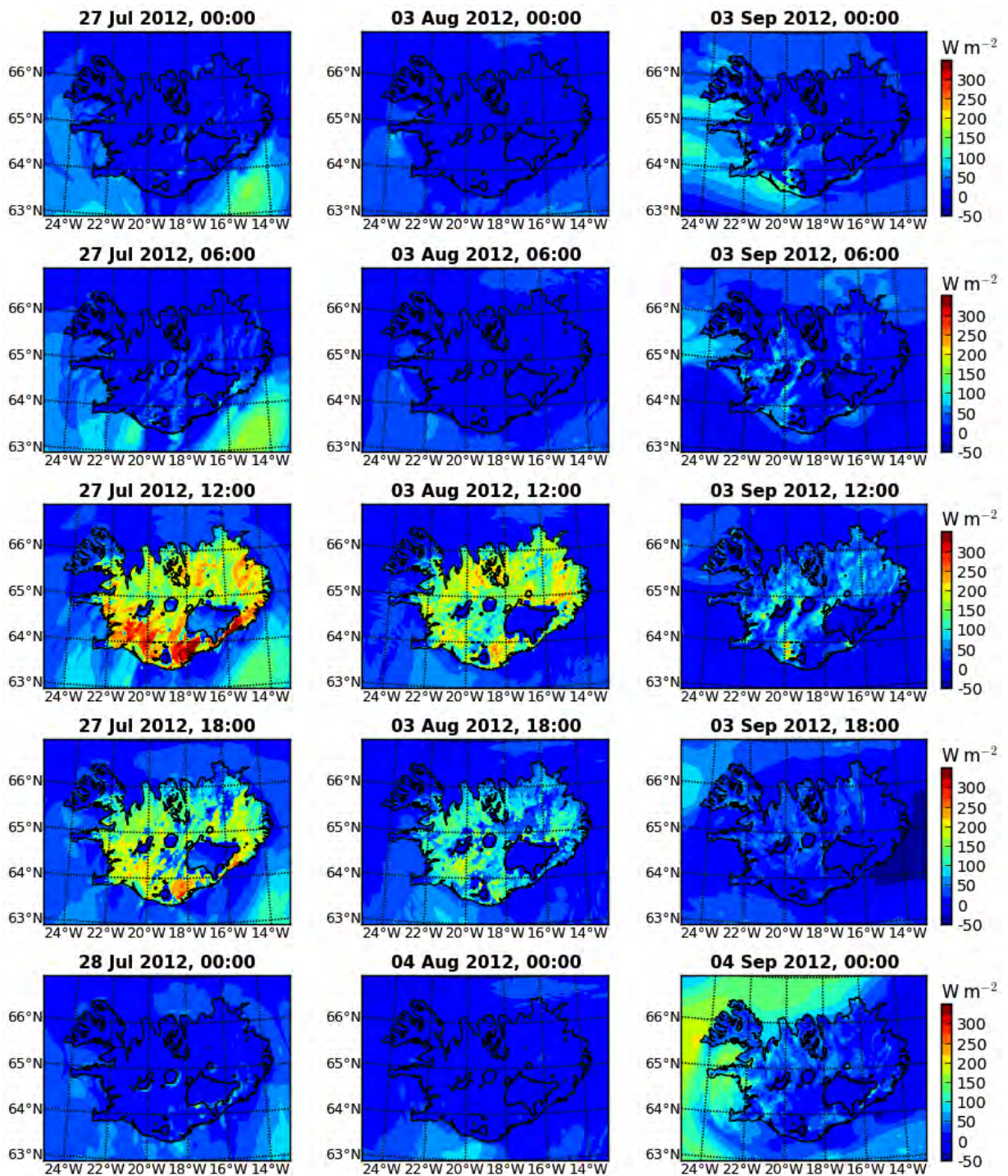


Figure 11. Upward latent heat flux from the ground, based on HARMONIE model simulations.

## 5 Net energy budget at the surface

The net surface energy budget, i.e., the total energy retained by the land or the ocean, is given by the sum of net downward short- and longwave radiation fluxes (Section 3), minus the sum of upward sensible and latent heat fluxes (Section 4), and is shown in Figure 12.

During the night, the net energy budget is predominantly negative, with only few regions of small positive energy balance due to sensible heat fluxes. After sunrise, the net energy budget quickly becomes positive, with highest values over cloud-free ocean areas and lakes. Despite reduced net shortwave radiation fluxes, compared with the snow-free surrounding regions, the net energy balance over the glaciers is positive during the day, due to reduced longwave radiation and latent heat losses, and small downward sensible heat fluxes. This excess energy then becomes available for melting of surface snow.

The energy needed to melt a given mass of snow,  $m_s$ , is given by

$$E = m_s L_f , \quad (1)$$

where  $L_f = 334,000 \text{ J kg}^{-1}$  is the latent heat of fusion. With an hourly change in snow water equivalent due to melting,  $d\Delta_{\text{melt}}$ , the amount of energy absorbed by the snowpack, per hour and unit area (energy flux), is given by

$$F = \rho_w d\Delta_{\text{melt}} L_f , \quad (2)$$

where  $\rho_w = 1 \text{ kg m}^{-3}$  is the density of liquid water. Hourly snow melt is calculated as the difference between the potential and the actual snow water equivalent at the end of each hour,  $d\Delta_{\text{melt}} = \Delta_{\text{pot}} - \Delta_{\text{act}}$ . The potential snow depth at the end of each hour is obtained by adding the total hourly solid precipitation (snow plus graupel) to the snow depth at the beginning of the hour, and subtracting the accumulated sublimation during that hour.



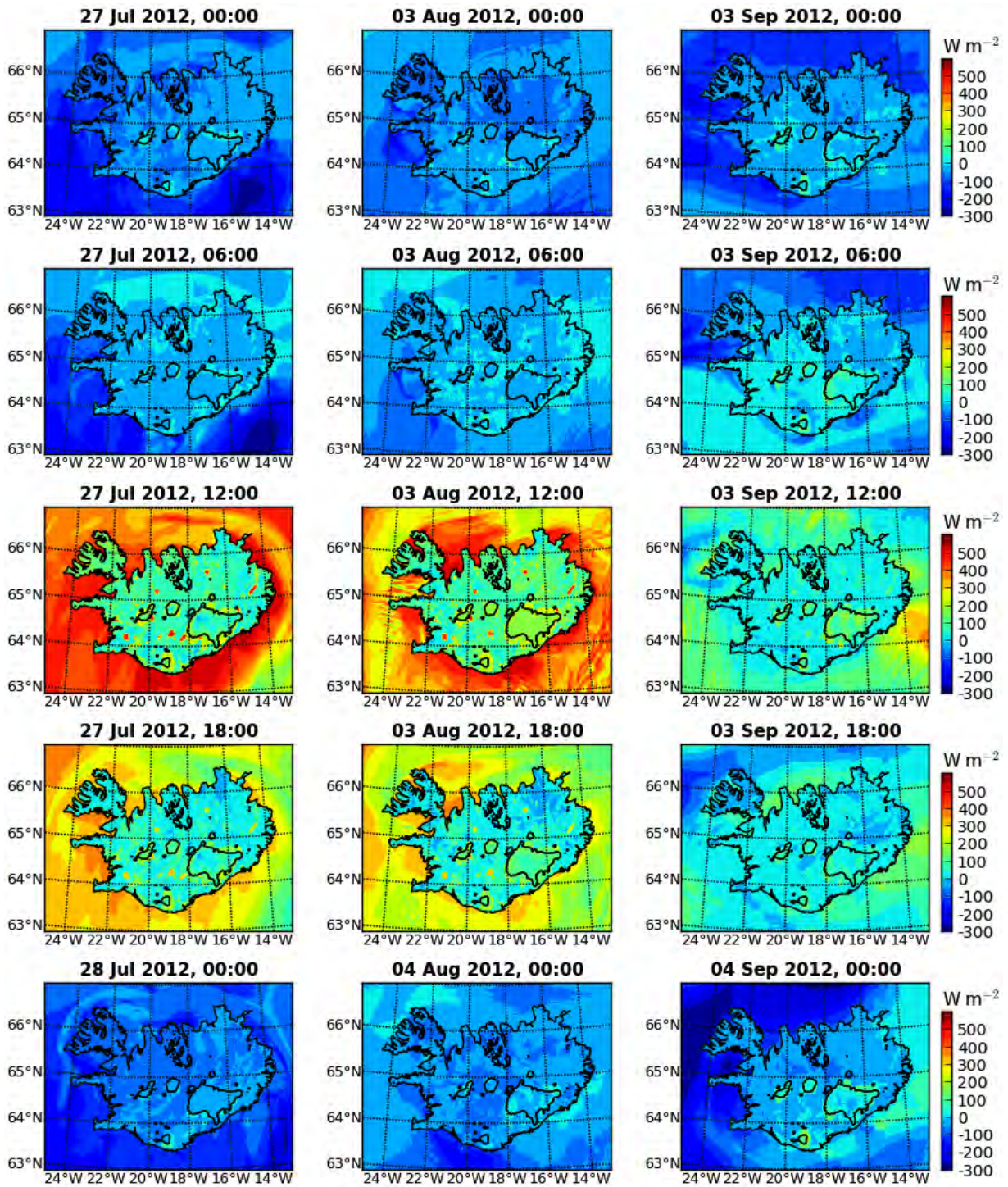


Figure 12. Net downward energy flux at the surface, without snowmelt, based on HARMONIE model simulations. Times are in UTC (local time). Terrain elevation contour lines are drawn at 1000 mASL, indicating roughly the extent of the glaciers.

The recalculated net surface energy budget, including also latent heat fluxes due to melting, is shown in Figure 13. To limit the range of values, the ocean area has been excluded. The values there are unchanged from Figure 12. While over the snow-free land area, and especially over lakes, the net energy flux can exceed  $200 \text{ W m}^{-2}$ , over the glaciers, it is limited to a maximum of zero, indicating that, as long as snow is present, all excess energy from radiation and heat fluxes is used for heating of the snowpack and subsequent melting.

Due to the variability in cloud cover characteristics (vertical thickness, height and type of clouds), as well as the shifting locations of clear-sky and overcast conditions over inhomogeneous ground (with varying elevation and thermodynamic or radiative properties), large temporal fluctuations in the daily energy budget can be expected at specific locations, or on average over the entire land area. To reduce these influences, the average net energy budget at the surface (excluding snowmelt and heat fluxes into the snow-free ground) is calculated separately for instances during which, at any given grid point, the sky is either clear (with a cloud cover of at most 1%), or overcast (with a cloud cover of at least 99%). As shown in Section 3, high-level clouds have a very limited impact on the surface radiation budget, and are therefore excluded. At each grid point, the total cloud cover is then determined as either the low- or mid-level cloud cover, depending on which is greater. In addition to cloud conditions, over land (excluding inland waterbodies), a distinction is made between snow-free and snow-covered regions. Since there is no sea ice within the model domain, over the ocean, the only distinction is made between cloudy and overcast conditions. In late summer and early autumn, snow is also limited to elevations above 1000 mASL, whereas snow-free areas are exclusively below that altitude. Therefore, implicit in the distinction between snow-covered and snow-free land areas is a difference in elevation. Due to this height difference alone, lower temperatures are to be expected over snow-covered regions, with reduced upward longwave radiation fluxes.



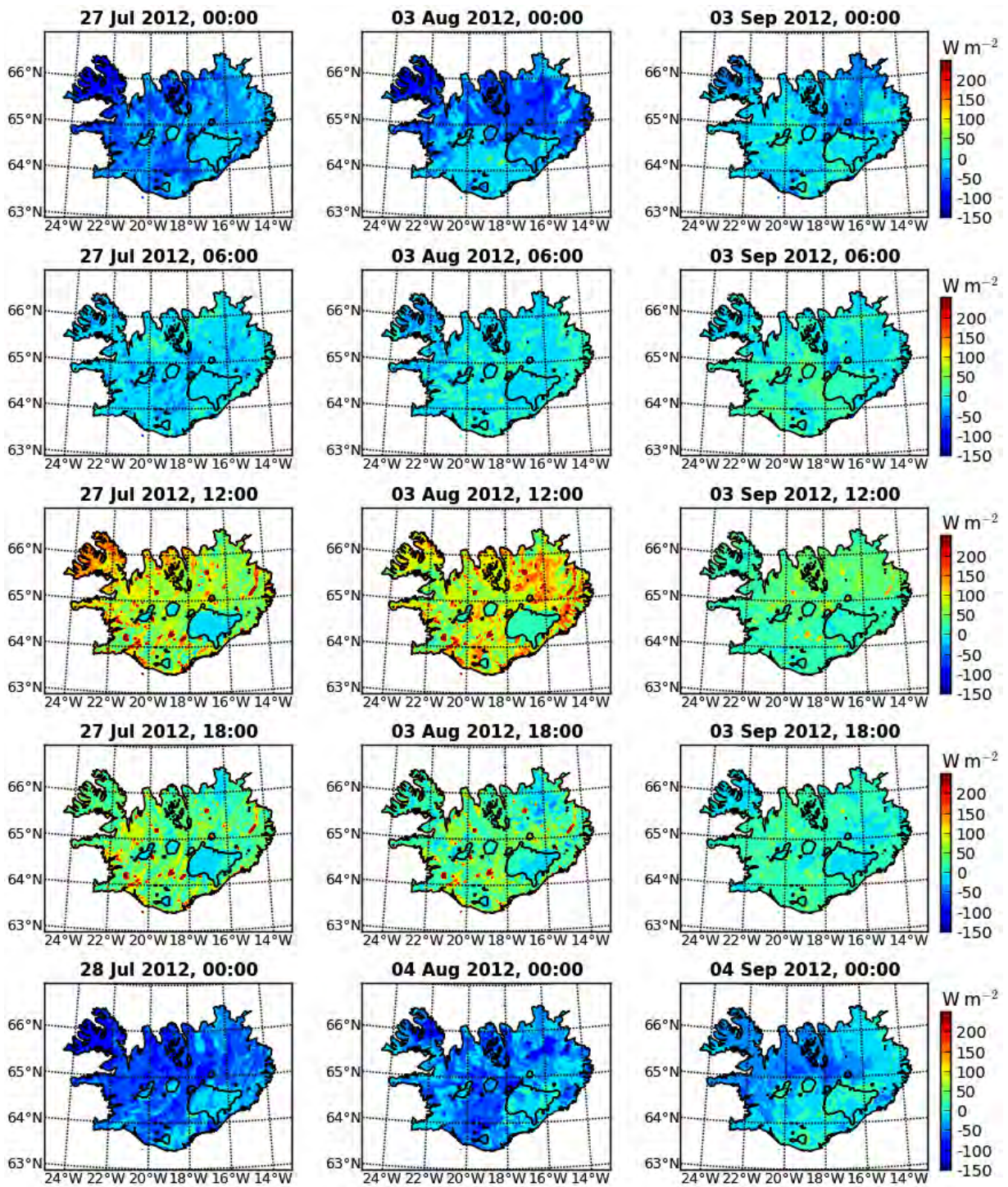


Figure 13. Net downward energy flux at the surface, with snowmelt, based on HARMONIE model simulations.

Average downward radiation and heat fluxes on 27 July are shown in Figures 14 and 15, for the land and ocean areas, respectively. From around midnight until sunrise, the average net energy balance over all three surface types (snow-free land, snow, and ocean) is negative, although over snow, nighttime energy loss is reduced, and near zero under overcast conditions. Over snow-free or snow-covered land, nighttime longwave radiation losses under clear skies are somewhat offset by downward sensible heat fluxes. Over the ocean, on the other hand, the negative net energy balance at night is increased further by both sensible and latent heat losses. After sunrise, as incoming shortwave radiation increases, the average net energy balance over all surface types becomes positive, even with overcast skies. Over snow-free land, this is despite the fact that, as convection sets in, there is an increased daytime loss of energy due to increased heat fluxes away from the surface, together with an increase in longwave radiation losses. Over snow, the increase in daytime surface temperature is limited by the conversion of part of the incoming solar energy into latent heat through the process of melting. Under either clear or overcast skies, diurnal changes in longwave radiation losses are therefore small. Similarly, due to the thermal inertia of water, sea surface temperature varies little over the course of a day, resulting in only small diurnal changes in net longwave radiation and heat fluxes over the ocean. Over snow-free land, regardless of cloud conditions, the incoming and outgoing energy fluxes are essentially balanced over the course of the day. Over snow, under both clear and overcast skies, the peak in net shortwave radiation flux is reduced by more than  $200 \text{ W m}^{-2}$ , compared with snow-free regions. However, the increased losses in shortwave radiation are overcompensated by reduced longwave radiation losses during the day, together with a reduction of heat losses, and even a positive sensible heat flux under clear skies. This leads to an overall positive net daily energy balance over snow.

There are large differences in the daily net energy received by either weakly or strongly reflecting surfaces. Over the ocean, especially under overcast conditions, the net energy balance is primarily determined by the incoming shortwave radiation. Due to the low albedo, the net shortwave flux peaks at more than twice the value over snow with clear skies, and almost four times the value over snow with overcast conditions. Throughout the day, almost three times the net shortwave radiation is received as over snow-covered surfaces, whereas longwave radiation losses are similar. Despite slightly increased losses due to heat fluxes, the net daily energy received over the ocean is twice to three times as high as over the glaciers.

Differences in net daily energy fluxes between clear-sky and overcast conditions, received over the same surface type, are smaller than between different surface types under the same cloud conditions. This is due to the partial balance between increased shortwave radiation gain and longwave radiation losses under clear skies, compared with overcast conditions.



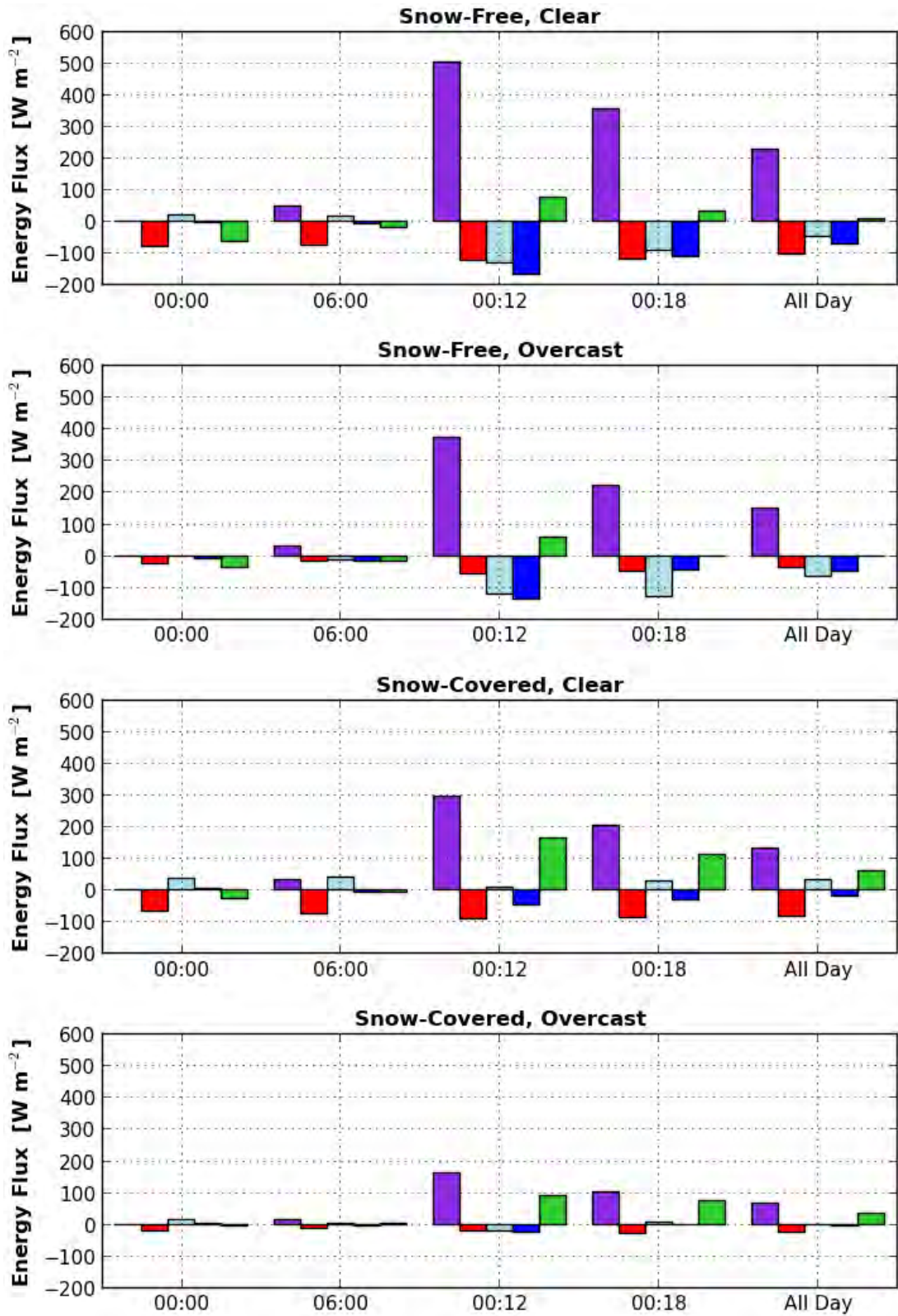


Figure 14. Average downward energy fluxes on 27 July 2012, for different surface types and cloud conditions: shortwave radiation (violet bars), longwave radiation (red bars), sensible heat (light blue bars), latent heat (medium blue bars), and total energy (green bars).

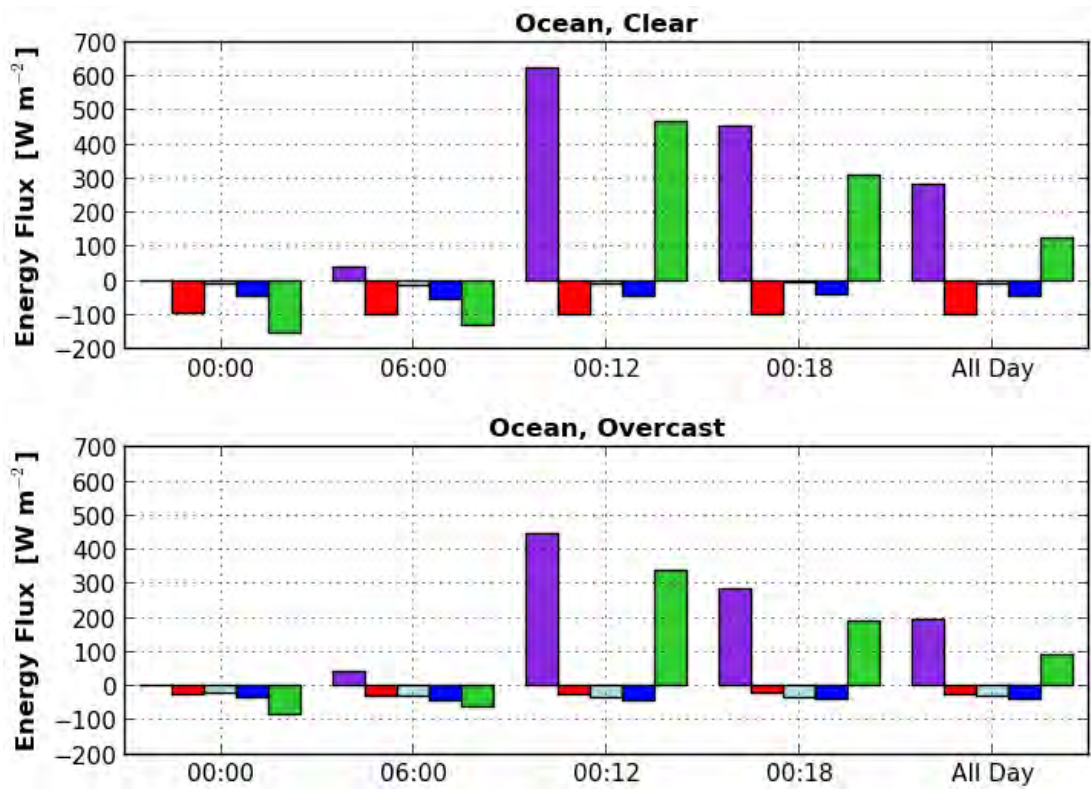


Figure 15. Average downward energy fluxes on 27 July 2012 over the ocean, and for different cloud conditions: shortwave radiation (violet bars), longwave radiation (red bars), sensible heat (light blue bars), latent heat (medium blue bars), and total energy (green bars).

A comparison of 27 July with the other two cases is complicated by the fact that, despite generally cloudy conditions on 3 August, only few clouds existed over snow-covered regions. On the other hand, on 3 September, only few grid points can be found without complete cloud cover. Therefore, only clear-sky conditions are considered for 3 August, and only overcast conditions for 3 September.

Radiation and heat fluxes over different surface types and under clear-sky conditions on 3 August are shown in Figure 16. Diurnal cycles in radiation and heat fluxes are qualitatively similar to the clear-sky conditions on 27 July. However, consistent with the decrease in solar altitude angle (see Table 1), net shortwave radiation fluxes are lower by 4 – 5%. Net longwave radiation fluxes are not significantly different over snow-free ground and the ocean, but are reduced by about 10 – 20 W m<sup>-2</sup> over snow. For sensible and latent heat fluxes, differences are unsystematic and within 30 W m<sup>-2</sup>.

For 3 September, results are shown in Figure 17. There are considerable differences compared with the earlier cases. These are partly due to the difference in solar altitude angle. However, even if the net shortwave radiation flux on 3 September is multiplied by the ratio of intensities on 27 July and 3 September (0.70 / 0.53; see Table 1), the rescaled flux maximum at noon on 3 September is reduced by a factor of 4.0 compared with 27 July over snow-free regions, by a factor of 2.6 over snow, and by a factor of 2.7 over the ocean. This demonstrates the effects of the denser cloud layer in the model. The thicker clouds also affect the diurnal cycle of net longwave radiation fluxes, limiting losses compared with earlier cases, and even contributing to positive net fluxes during the day over snow-covered regions. Throughout 27 July, sensible heat flux over snow-free ground is directed upwards to the atmosphere, supporting convection. By contrast, on 3 September, sensible heat fluxes are in the opposite direction. This distinction between convective and stable boundary layers is consistent with the observed low- and mid-level cloud types on the two days (see Section 2), with cumuliform clouds dominating on 27 July, and stratiform clouds dominating on 3 September. The high relative humidity on 3 September (see Figure 18) causes an inversion of the usual vertical vapour pressure gradient over snow-covered regions, with latent heat fluxes during that day directed from the atmosphere to the ground.

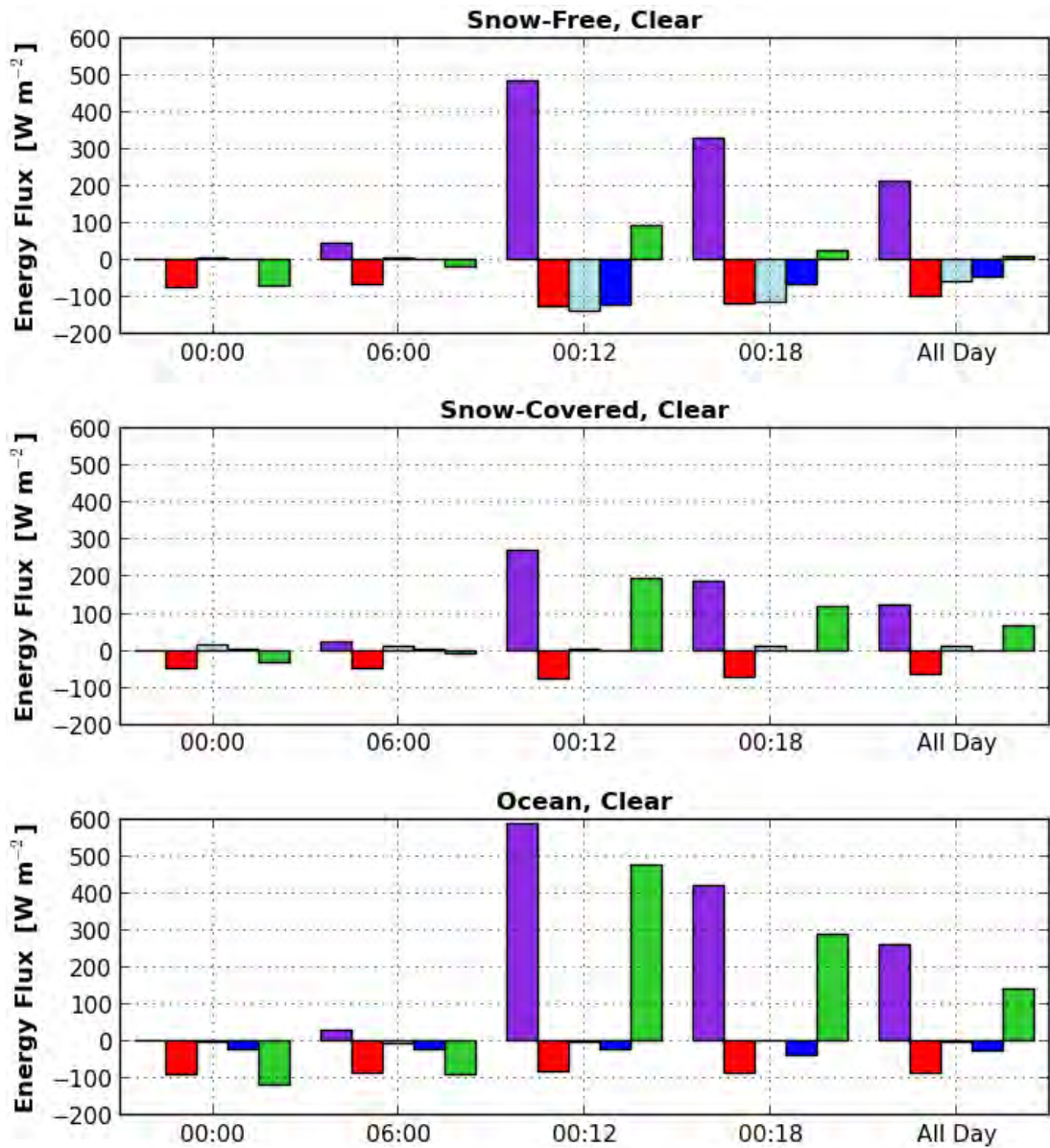


Figure 16. Average downward energy fluxes on 3 August 2012, for different surface types and cloud conditions: shortwave radiation (violet bars), longwave radiation (red bars), sensible heat (light blue bars), latent heat (medium blue bars), and total energy (green bars).



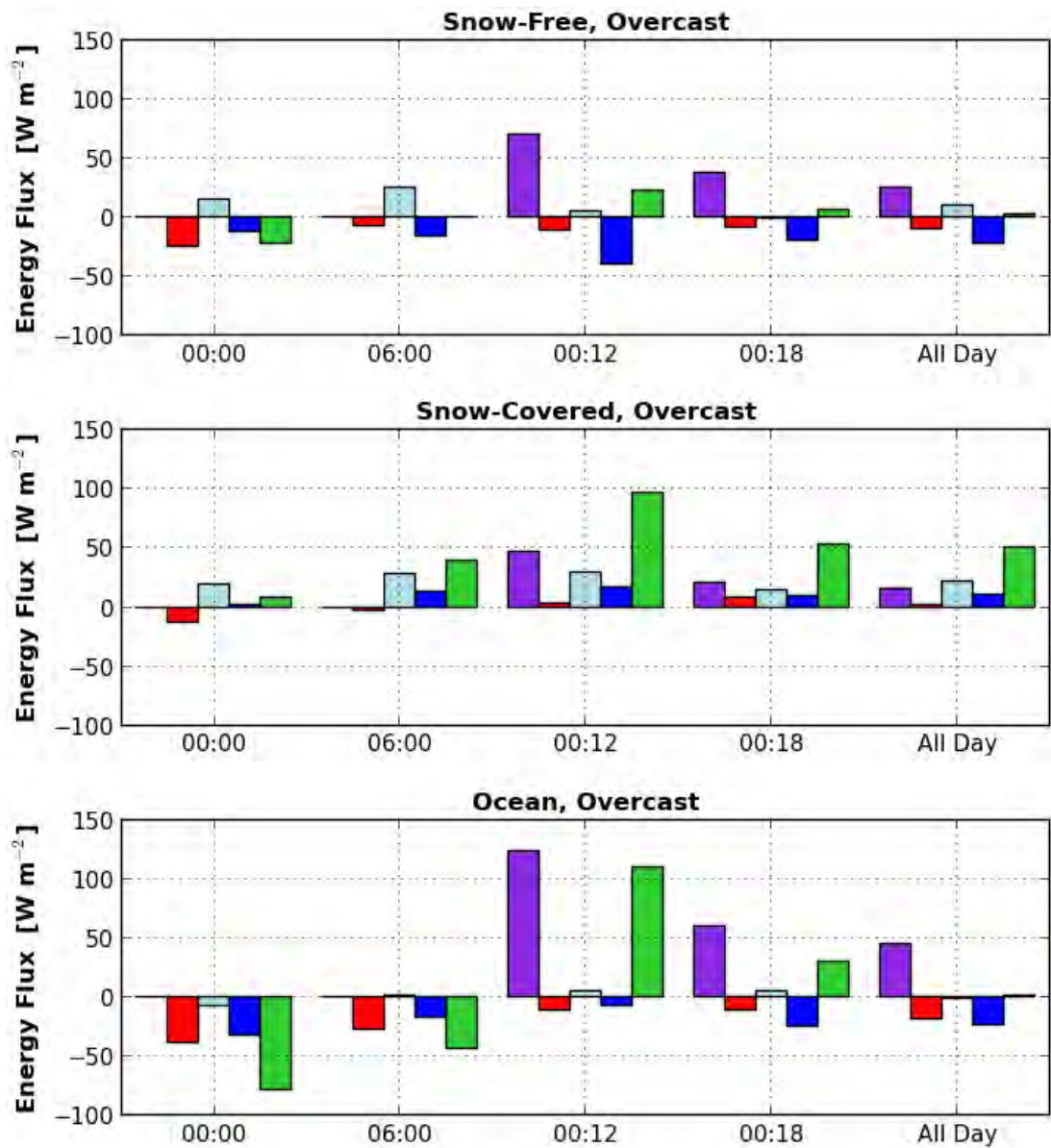


Figure 17. Average downward energy fluxes on 3 September 2012, for different surface types and cloud conditions: shortwave radiation (violet bars), longwave radiation (red bars), sensible heat (light blue bars), latent heat (medium blue bars), and total energy (green bars).

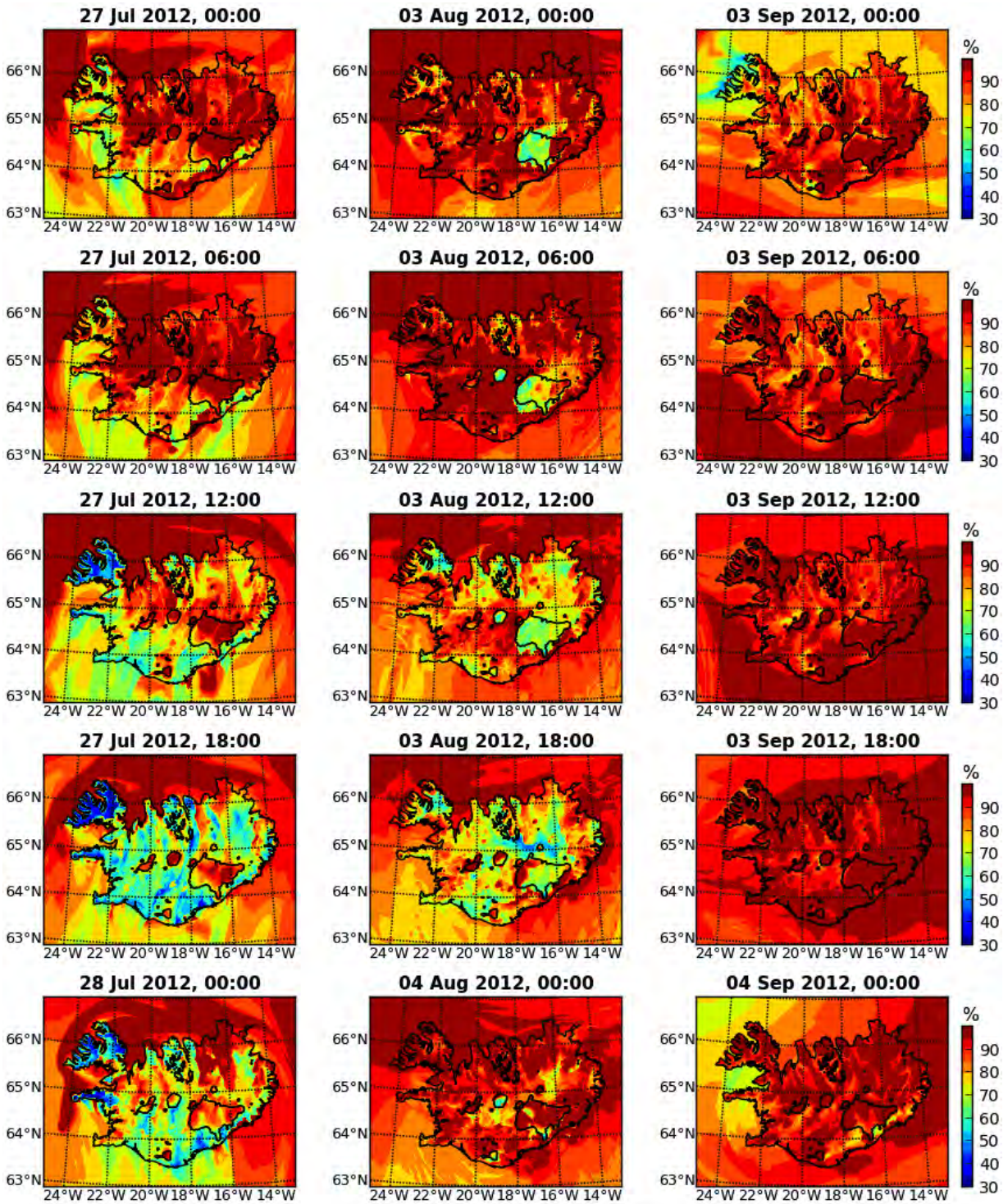


Figure 18. Relative humidity at 2 mAGL, based on HARMONIE model simulations.

## 6 Impact of glaciers on surface winds

With the same large-scale weather conditions, the presence of glaciers – and more generally, any snow-covered region in the interior of Iceland – has a significant impact on the thermodynamic properties of the boundary-layer atmosphere in HARMONIE model simulations.

Due to increased longwave radiation losses, and reduced sensible heat fluxes over snow-covered regions (see Sections 3 and 4), 2-m air temperature is decreased by several degrees over snow-covered regions, compared with the “no snow” runs (not shown). Since radiative cooling is greatest under clear skies, the largest differences in 2-m temperature of up to 8 K, between the “no snow” and “snow on glaciers” runs, occurred on 3 August.

Due to reduced latent heat fluxes over snow-covered regions (see Section 4), 2-m specific humidity is decreased by up to 4 g kg<sup>-1</sup> near the edges of Vatnajökull (not shown). However, combined with the effects of decreased temperature, 2-m relative humidity is increased over the snow-covered regions by more than 30% (not shown).

As a result of the decreased boundary-layer temperatures, mean sea level air pressure may be increased by more than 3 hPa over glaciers, compared with the same<sup>1</sup> but snow-free terrain (see Figure 19). As for 2-m air temperature, the largest differences are found on 3 August. The pressure difference induced by the snow cover over Vatnajökull on that day is approximately of the same magnitude as the large-scale pressure difference across the entire island (see again Figure 2).

Related to these changes in thermodynamic properties, there is a dynamic response of the boundary-layer atmosphere. The increased pressure at high elevations causes a strengthening of divergent downslope and offshore winds by up to 8 m s<sup>-1</sup>. In Figure 20, this is shown based on differences in the meridional wind component between the “snow on glaciers” and “no snow” runs. The largest differences are found along the northern edge of Vatnajökull, where the contrast between the snow-covered and the snow-free region (characterised as dark bare rocks in the model) is greatest. On 27 July, at 0 and 18 UTC, the large differences off the south coast are due to small east-west shifts of the anticyclonic return circulation in the wake of the island, with northerly prevailing winds.

---

<sup>1</sup>The snow cover homogeneously increases the terrain elevation by only 0.5 m, without changing the shape of the orography.



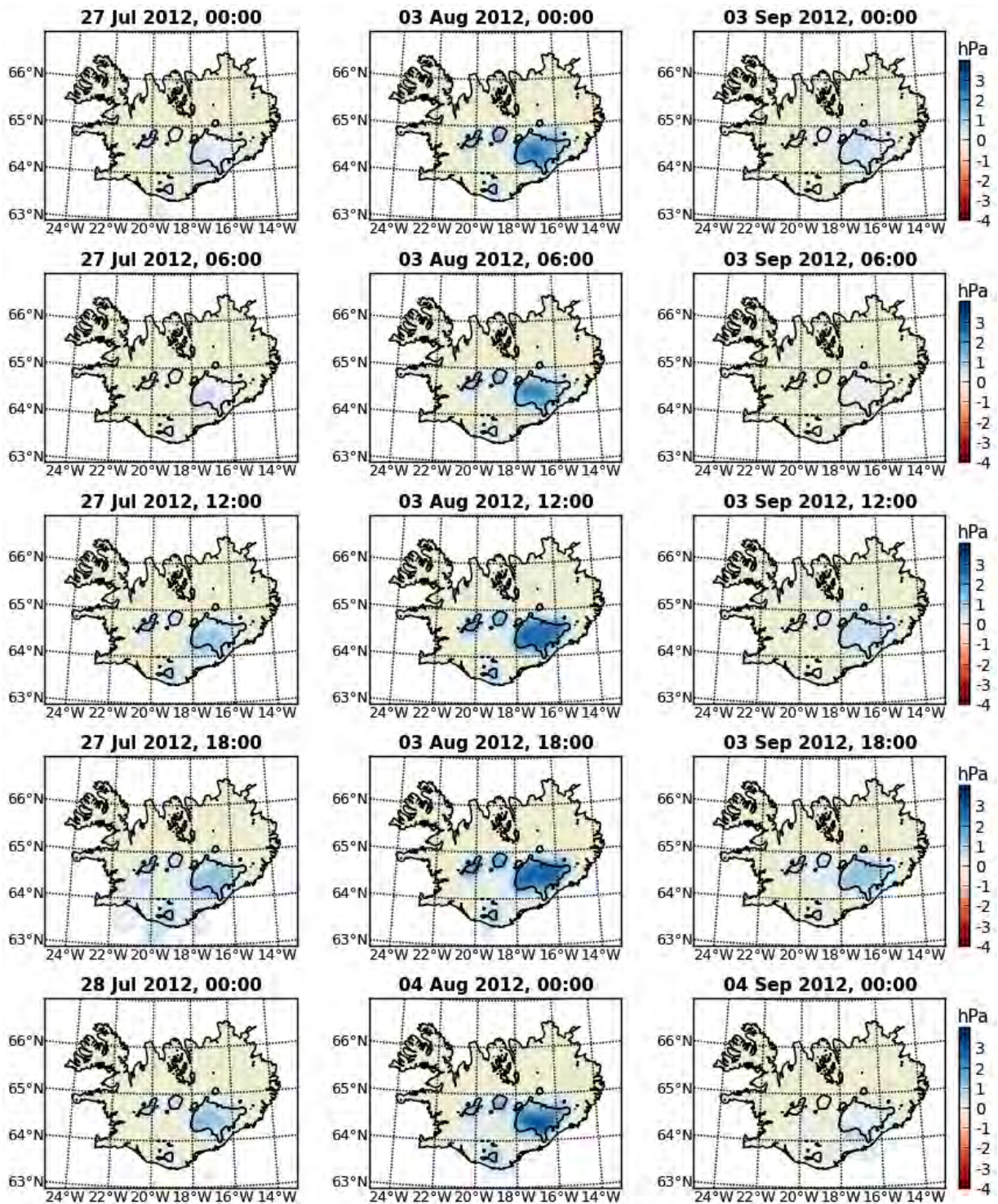


Figure 19. Differences in mean sea level air pressure between the “snow on glaciers” and “no snow” HARMONIE model simulations (“snow” minus “no snow”). Times are in UTC (local time). Terrain elevation contour lines are drawn at 1000 mASL, indicating roughly the extent of the glaciers.



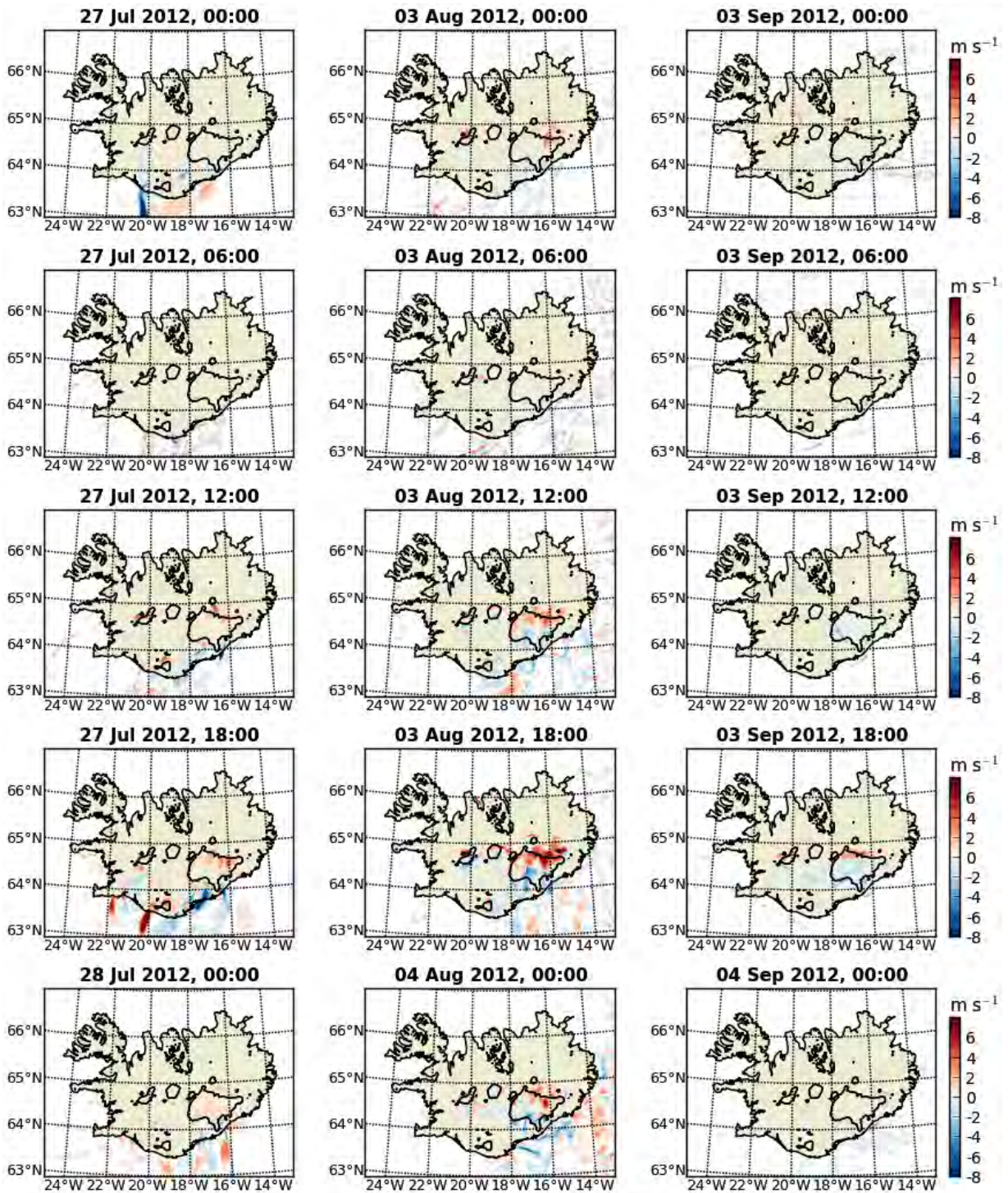


Figure 20. Differences in the meridional wind component at 10 mAGL between the “snow on glaciers” and “no snow” HARMONIE model simulations (“snow” minus “no snow”).

## 7 Conclusion

In this study, the sensitivity of the HARMONIE mesoscale weather prediction model to changes in snow and cloud cover has been investigated, based on case studies of three individual days in the late summer and early autumn of 2012, with a particular emphasis on radiation and heat fluxes, as well as on the overall energy balance.

The three days (27 July, 3 August, and 3 September) were associated with different large-scale weather patterns, and characterised by different cloud conditions over Iceland, which were generally well simulated by HARMONIE, although for the first two cases, small precipitation events and mid-level cloud cover were underestimated.

As is to be expected, HARMONIE simulations of radiation and heat fluxes at the Earth's surface are significantly affected by the transmittance of the atmosphere, and by surface reflectivity.

For 27 July, spatially averaged noontime energy fluxes are summarised in Table 2, over different surface types and with different cloud conditions. For a given incident flux of solar radiation, the net downward shortwave radiation flux at the surface varies between a minimum of 14% over snow-covered land with overcast conditions, and a maximum of 66% over the ocean with clear-sky conditions. This incoming radiation at the Earth's surface is then converted to other forms of energy, with a distribution in percent of the net solar radiation flux, which again depends on the surface type and cloud conditions. Compared with shortwave radiation, longwave radiation fluxes are less dependent on the presence or absence of snow on the ground, and more on cloud conditions. Relative net longwave radiation losses vary between a minimum of 5% over the ocean with overcast conditions, and a maximum of 36% over the glaciers with clear skies. Sensible heat fluxes remove between 2% (cloud-free ocean) and 36% (overcast snow-free land) of the incoming solar energy. Over the glaciers, on the other hand, under clear conditions, the snowpack gains a further 6% of the net downward shortwave radiation flux by sensible heat transfer from the atmosphere. Relative latent heat fluxes show a similar spatial pattern as sensible heat fluxes, with a minimum of 8% over the cloud-free ocean, and a maximum of 36% over the overcast snow-free land. At local noon (about 1.5 hours prior to solar noon), the net downward total energy flux is positive across the model domain. It is largely unaffected by cloud conditions, but significantly depends on surface type. The lowest values of 14 – 15% of the net

*Table 2. Noontime downward shortwave radiation flux, upward longwave radiation flux, and upward sensible and latent heat fluxes in  $W m^{-2}$  at the Earth's surface on 27 July 2012 for different surface types and cloud conditions. Percentages in parentheses are relative to the incident solar radiation flux at the top of the atmosphere ( $0.70 \times 1360 W m^{-2}$ , see Table 1) for  $SW_{\downarrow}$ , and relative to  $SW_{\downarrow}$  for the other fluxes.*

	SW $\downarrow$	LW $\uparrow$	SH $\uparrow$	LH $\uparrow$	Net $\downarrow$
Snow-free land & Clear	502 (53%)	128 (25%)	138 (27%)	165 (33%)	71 (15%)
Snow-free land & Overcast	335 (35%)	46 (14%)	119 (36%)	121 (36%)	49 (14%)
Snow-covered & Clear	262 (27%)	95 (36%)	-15 (-6%)	43 (16%)	139 (54%)
Snow-covered & Overcast	132 (14%)	19 (15%)	22 (17%)	21 (16%)	70 (52%)
Ice-free ocean & Clear	624 (66%)	100 (16%)	11 (2%)	49 (8%)	464 (74%)
Ice-free ocean & Overcast	430 (45%)	24 (5%)	36 (8%)	45 (11%)	325 (76%)

incoming radiation flux are found over the snow-free land area. Over the glaciers, the relative (and absolute) net energy received by the ground increases to 52 – 54%, due to the lower temperatures, and therefore reduced longwave radiation and heat losses. It is increased even more to 74 – 76% over the ocean, by further reducing longwave radiation and heat losses.

The spatially averaged daily mean energy fluxes on 27 July are summarised in Table 3. As for the conditions at noon, there is a wide range in the absolute values, as well as the relative redistribution into different forms of energy. There are no local measurements to properly validate the results. However, a few observation-based studies of the surface energy budget at high latitudes can be referred to for comparison. Westermann, Lüers, Langer, Piel, and Boike (2009) studied radiation and heat fluxes over a permafrost region in Svalbard, described as hilly tundra, with sparse vegetation, exposed soil, and bare rocks. The region is therefore geographically similar to the unglaciated terrain in Iceland. However, at 79°N, it is situated at a significantly higher latitude, which needs to be taken into account, when comparing the incoming solar energy. The average net downward shortwave radiation flux at the Earth’s surface during July – August 2008 was found to be 122 W m<sup>-2</sup>. With a sun altitude angle of 28.86 degrees at solar noon on 1 August 2008, the net shortwave radiation flux, rescaled to the central latitude of Iceland (65°N), is given by 178 W m<sup>-2</sup>, and is therefore within the range of overcast and clear-sky values over the snow-free land in Iceland, as simulated by HARMONIE. Westermann et al. (2009) also found that 35% of the incoming solar energy are lost through longwave radiation, which again is between the overcast and clear-sky values simulated for Iceland. However, at 18%, the sensible and latent heat losses are significantly lower than the range of values found in Iceland, resulting in 29% of the incoming energy flux to be absorbed by the ground, while (on 27 July 2012) the net energy balance over the snow-free ground in Iceland fluctuates around zero. This might be due to the melting of ground ice in the active layer above the permafrost of the Svalbard site. However, a longer data period is required for Iceland, to give a more definitive answer. Giesen, Andreassen, Oerlemans, and van den Broeke (2014) found that the July – August average of the net downward shortwave radiation flux at the surface of three glaciers in Norway ranged between 70 – 125 W m<sup>-2</sup>, based on the actually measured values, or between 80 – 120 W m<sup>-2</sup>, based on values rescaled to 65°N. The range of overcast and clear-sky values over the Icelandic glaciers is therefore about 15 W m<sup>-2</sup> lower, and a longer model data record is necessary to determine

*Table 3. Daily mean downward shortwave radiation flux, upward longwave radiation flux, and upward sensible and latent heat fluxes in W m<sup>-2</sup> at the Earth’s surface on 27 July 2012 for different surface types and cloud conditions. Percentages in parentheses are relative to the scaled incident solar radiation flux at the top of the atmosphere (0.70×1360 W m<sup>-2</sup>, see Table 1) for SW↓, and relative to SW↓ for the other fluxes.*

	SW↓	LW↑	SH↑	LH↑	Net↓
Snow-free land & Clear	228 (24%)	103 (45%)	48 (21%)	71 (31%)	6 (3%)
Snow-free land & Overcast	137 (14%)	29 (21%)	67 (49%)	45 (33%)	-4 (-3%)
Snow-covered & Clear	116 (12%)	87 (75%)	-38 (-33%)	19 (16%)	48 (42%)
Snow-covered & Overcast	54 (6%)	18 (34%)	3 (6%)	6 (11%)	27 (49%)
Ice-free ocean & Clear	282 (30%)	99 (35%)	10 (4%)	48 (17%)	125 (44%)
Ice-free ocean & Overcast	186 (20%)	22 (12%)	32 (17%)	40 (22%)	92 (49%)

whether this also holds for monthly averages. Based on data from an ongoing IMO reanalysis project, this will be the subject of future analyses.

## References

- Brousseau, P., Berre, L., Bouttier, F., & Desroziers, G. (2011). Background-error covariances for a convective-scale data-assimilation system: AROME – France 3D-Var. *Q. J. R. Meteorol. Soc.*, *137*, 409-422.
- Giesen, R. H., Andreassen, L. M., Oerlemans, J., & van den Broeke, M. R. (2014). Surface energy balance in the ablation zone of Langfjordjøkelen, an arctic, maritime glacier in northern Norway. *J. Glaciol.*, *60*(219), 57-70.
- Seity, Y., Brousseau, P., Malardel, S., Hello, G., Bénard, P., Bouttier, F., . . . Masson, V. (2011). The AROME-France convective-scale operational model. *Mon. Wea. Rev.*, *139*, 976-991.
- Westermann, S., Lüers, J., Langer, M., Piel, K., & Boike, J. (2009). The annual surface energy budget of a high-arctic permafrost site on Svalbard, Norway. *The Cryosphere*, *3*, 245-263.